



## **Magnetite magnetosome biomineralization in Magnetospirillum magneticum strain AMB-1: A time course study**

Lucas Le Nagard, Xiaohui Zhu, Hao Yuan, Karim Benzerara, Dennis A Bazylinski, Cecile Fradin, Adrien Besson, Sufal Swaraj, Stefan Stanescu, Rachid Belkhou, et al.

### **► To cite this version:**

Lucas Le Nagard, Xiaohui Zhu, Hao Yuan, Karim Benzerara, Dennis A Bazylinski, et al.. Magnetite magnetosome biomineralization in *Magnetospirillum magneticum* strain AMB-1: A time course study. *Chemical Geology*, 2019, 530, pp.119348. <10.1016/j.chemgeo.2019.119348>. <hal-02411165>

**HAL Id: hal-02411165**

**<https://hal.science/hal-02411165v1>**

Submitted on 14 Dec 2019

**HAL** is a multi-disciplinary open access archive for the deposit and dissemination of scientific research documents, whether they are published or not. The documents may come from teaching and research institutions in France or abroad, or from public or private research centers.

L'archive ouverte pluridisciplinaire **HAL**, est destinée au dépôt et à la diffusion de documents scientifiques de niveau recherche, publiés ou non, émanant des établissements d'enseignement et de recherche français ou étrangers, des laboratoires publics ou privés.



HAL Authorization

**Magnetite Magnetosome Biomineralization in *Magnetospirillum magneticum* strain AMB-1: a Time Course Study**

Lucas Le Nagard,<sup>1,+</sup> Xiaohui Zhu,<sup>2,#</sup> Hao Yuan<sup>2</sup>, Karim Benzerara,<sup>3</sup> Dennis A. Bazylinski,<sup>4</sup> Fradin<sup>1</sup>, Adrien Besson,<sup>5</sup> Sufal Swaraj,<sup>5</sup> Stefan Stanescu,<sup>5</sup> Rachid Belkhou<sup>5</sup> and Adam P. Hitchcock<sup>1,2,\*</sup>

<sup>1</sup>. Dept. of Physics & Astronomy, McMaster University, Hamilton, Canada  
<sup>2</sup> Dept. Chemistry & Chemical Biology, McMaster University, Hamilton, Canada  
<sup>3</sup> Institut de Minéralogie, de Physique des Matériaux et de Cosmochimie, Sorbonne Université, UMR CNRS 7590, Muséum National d'Histoire Naturelle, Paris, France  
<sup>4</sup> School of Life Sciences, University of Nevada-Las Vegas, Las Vegas, USA  
<sup>5</sup> Synchrotron SOLEIL, St. Aubin, France

**Abstract:** Magnetotactic bacteria are a highly studied group of diverse prokaryotes that biomineralize chains of magnetosomes, single domain, single crystal magnetic nanoparticles of magnetite or greigite, enclosed by a lipid bilayer membrane whose synthesis is under strict control. In addition to characterizing the genetics and physicochemical properties of both and uncultured environmental species, there have been a number of investigations using a time course approach to determine the chemical pathway of magnetite biomineralization in these organisms. In time course studies, cells of MTB are typically grown in the absence of iron so cannot make magnetite, and then provided with iron in culture medium which initiates the biomineralization of magnetosome chains over a subsequent time period. Results from previous time course studies are not consistent with one another, differing with regard to the nature of chemical intermediates and the rate of establishment of magnetosome chains. In this work we report a time course study of *Magnetospirillum magneticum* strain AMB-1 over a 48 hour (h) period, using transmission electron microscopy (TEM) and soft X-ray scanning transmission X-ray microscopy (STXM) at the Fe L-edge. STXM provides capability to measure X-ray absorption spectra (XAS) and map chemical species with ~25 nm spatial resolution and thus detailed results on the chemistry of individual particles in single cells. An evolution of the iron

oxide speciation, from a more Fe(III)-rich species, possibly  $\alpha$ -hematite ( $\text{Fe}_2\text{O}_3$ ), to magnetite ( $\text{Fe}_3\text{O}_4$ ), was observed in the early stages, with evidence for the presence of the Fe(III)-rich character persisting up to 24 h. The spectromicroscopy (X-ray absorption, XAS and X-ray magnetic circular dichroism, XMCD) and TEM results show that biomineralization occurs in a stepwise fashion. First, very small particles, with no measurable magnetization, are produced at different sites in the cell without significant chain formation. The Fe  $L_3$  spectra of these early stage particles typically differ from magnetite with an additional signal at 708.4 eV that is consistent with  $\alpha$ -hematite. By 6-8 h the particles are more numerous, partial chain formation is evident, and the  $L_3$  spectrum is very similar to that of magnetite. By 24 h particles-in-chains are the dominant motif and magnetism with the moment along the chain is established. By 48 h the cells are essentially the same as cells grown in Fe-rich medium.

**Keywords:** magnetotactic bacteria; *Magnetospirillum magneticum* strain AMB-1; biomineralization; time course; transmission electron microscopy; synchrotron spectro-microscopy; STXM; X-ray absorption; X-ray magnetic circular dichroism

**Highlights:**

- \* TEM and STXM study of magnetosome biomineralization in AMB-1 magnetotactic bacteria
- \* time course method: cells cultured without Fe; placed in normal medium; sampled at 0.15, 0.5, 1, 2, 4, 5.7, 8, 12, 24, 28 h
- \* TEM particle counts/cell; STXM measure Fe L X-ray absorption and X-ray magnetic circular dichroism
- \* Fe(III) rich precursor, possibly  $\alpha$ -hematite, observed in <8 h samples
- \* pure magnetite particles aligned in chains form by 12 hr; gaps and magnetic reversals persist at 48 h

Chemical Geology (submitted 19 June 2019; REVISION submitted 13 Sep 2019; final sun 19-Oct 20119)

File: AMB-1-time-course-STXM-revised2.doc

**Last changed: 19 Oct 2019**

<sup>+</sup> present address: School of Physics & Astronomy, The University of Edinburgh, Scotland

# present address: School of Environmental and Chemical Engineering, Shanghai University, 200444, Shanghai, China.

\* corresponding author. Email: [aph@mcmaster.ca](mailto:aph@mcmaster.ca)

## 1. Introduction

Magnetotactic bacteria (MTB) biomineralize intracellular, single-magnetic-domain, single-crystal, membrane- bounded magnetite ( $\text{Fe}_3\text{O}_4$ ) or greigite ( $\text{Fe}_3\text{S}_4$ ) nanoparticles known as magnetosomes (Bazylinski and Frankel 1995). Magnetosomes are generally organized as a chain or chains within the cell (Bazylinski 1999). In this arrangement, they function as a strong magnetic dipole, so the cell passively aligns along the Earth's geomagnetic field lines like a compass needle. Coupled with aerotaxis (chemotaxis to the concentration of  $\text{O}_2$ ), magneto-aerotaxis is believed to increase the efficiency of MTB in locating and maintaining their position at their optimal  $\text{O}_2$  concentration and redox poise for survival in sediments or stratified water columns (Bazylinski 1999). The optimal  $\text{O}_2$  concentration/redox conditions for most MTB appears to be at, or close to, the oxic-anoxic interface (OAI) (Faivre & Schuler 2008). MTB, which likely evolved in the mid-Archaeon, are of tremendous interest as possibly one of the earliest organisms on Earth capable of magnetic sensing and biomineralization (Lin *et al.* 2017). They are a superb 'laboratory' for dissecting controlled biomineralization. They significantly impact the magnetic properties of sediments (Chen *et al.* 2015), and are implicated in the geochemical cycles of phosphorus (Rivas *et al.* 2018, Schulz-Vogt *et al.* 2019) and iron (Lin *et al.* 2013, Lin *et al.* 2014, Chen *et al.* 2014, Amor *et al.* 2019). Through measurements of the iron content of single AMB-1 cells, Amor *et al.* (2019) showed that MTB absorb a significant fraction of the iron dissolved in their environment and thus play an important role in global iron distributions. Cells of a mutant lacking core genes for biomineralization also contained a significant (but decreased) amount of iron, indicating that magnetosomes are only one reservoir of iron among others in MTB.

The genetic control of magnetosome biomineralization is an active area of study. A conserved core of essential genes has been identified (Komeili *et al.* 2004, Jogler and Schüller, 2007, Arakaki *et al.* 2008, Murat *et al.* 2012). However, the chemical steps and reactions in magnetosome biomineralization are still not fully understood (Lefevre & Bazylinski, 2013). Several competing hypotheses exist. Frankel *et al.* (1983) reported that  $(\text{Fe}^{3+})_2\text{O}_3 \cdot 0.5\text{H}_2\text{O}$ , an

1  
2  
3  
4  
5 97 amorphous ferrihydrite, is formed first, and is then partially reduced and dehydrated to Fe<sub>3</sub>O<sub>4</sub>.  
6  
7 98 Faivre *et al.* (2007) did not observe any well-ordered, crystalline precursors in a time-resolved  
8  
9 99 Mössbauer study. They found that Fe<sup>2+</sup> or Fe<sup>3+</sup> was taken into the cell and converted into an  
10  
11 100 intracellular amorphous ferrous high-spin species, predominantly located in the magnetosome  
12  
13 101 membrane, along with ferritin. These then quickly co-precipitate to directly form Fe<sub>3</sub>O<sub>4</sub> within  
14  
15 102 magnetosome vesicles. In a recent ptychography study, Zhu *et al.* (2016) observed hematite  
16  
17 103 ( $\alpha$ -Fe<sub>2</sub>O<sub>3</sub>) in cells of *Magnetovibrio blakemorei* strain MV-1 which was interpreted to be a  
18  
19 104 possible precursor to magnetite in the formation of magnetite magnetosomes.

20  
21 105 Results from various time course studies of magnetite magnetosome synthesis in MTB are  
22  
23 106 summarized in **Supplemental Information Table S-1**. These studies all focused on either  
24  
25 107 *Magnetospirillum magneticum* strain AMB-1 or *Magnetospirillum gryphiswaldense* strain  
26  
27 108 MSR-1 as the model MTB for magnetite biomineralization. With some exceptions, there seems  
28  
29 109 to be a general consensus that:

30  
31 110 \* a lag phase occurs before particle formation, typically in the 0.5-2 hour (h) range (Li *et al.*  
32  
33 111 2009).

34  
35 112 \* crystal growth occurs in lipid bilayer membrane vesicles which are present prior to the  
36  
37 113 visible detection of crystals (Komeli *et al.* 2004).

38  
39 114 \* there is a period of time during which the mean size of the particles is in the  
40  
41 115 superparamagnetic size range, significantly smaller than that of mature magnetosomes, and  
42  
43 116 there is a broad size distribution (Firlar *et al.* 2016).

44  
45 117 \* the particles are poorly organized in the early stages of biomineralization but become  
46  
47 118 arranged in chains with more or less regular spacing, after a period of time which varies  
48  
49 119 considerably depending on the study (Heyen and Schüler 2003, Firlar *et al.* 2016), suggesting  
50  
51 120 that the temporal evolution depends on the culturing and growth conditions (growth phase,  
52  
53 121 O<sub>2</sub> concentration, temperature, etc).

\* after 24-48 h, the size and shape of individual particles and their organization in the cell approach that in magnetosomes present in stationary phase MTB grown with a major source of Fe.

\* the magnetic properties of particles produced in the early stages differ greatly. Staniland *et al.* (2007), using ensemble averaged Fe L-edge X-ray magnetic circular dichroism (XMCD), stated that a full XMCD response, and thus magnetic magnetite, was detected 15 minutes (m) after Fe-depleted cells were placed in a standard growth medium containing a major source of Fe. However, Faivre *et al.* (2007) only detected Mössbauer signal indicative of magnetite 95 m after incubation with iron. Similarly, Baumgartner *et al.* (2013), using magnetically induced differential light scattering, only found a magnetic response 80 m after incubation with Fe. Baumgartner *et al.* (2013) also used ensemble averaged X-ray absorption spectroscopy (XAS) to show that Fe K-edge features typical of magnetite only appeared after ~100 m, consistent with their magnetic measurements. Li *et al.* (2009), using temperature-dependent magnetometry, detected a magnetic response characteristic of magnetite (hysteresis and Verwey transition) 28 h after the start of the time course, which, unfortunately, was their first time data point. We note that the variation in magnetic results may simply reflect the use of different methods which have different spatial, concentration and magnetic field sensitivities.

\* there is an Fe(III)-rich intermediate to magnetite. While the presence of some type of Fe(III) in cells in the early stages of growth is a common observation, there is disagreement whether this is a single mineral precursor species with a unique chemical composition and structure, a mixture of species, or simply Fe(III) ions. Some report such precursors to be amorphous, others as crystalline. In some cases, this is reported as a surface  $\alpha$ -hematite layer (Staniland *et al.* 2007, Firlar *et al.* 2019). Using XAS, Fdez-Gubieda *et al.* (2013) identified phosphorus-rich ferrihydrite as a precursor of magnetite in MSR-1 but were unable to image the precursors with high resolution transmission electron microscopy (TEM). Using K-edge XAS and extended X-ray absorption fine structure (EXAFS) and a more complete set of

reference spectra, Baumgartner *et al.* (2013) concluded from spectra similar to those measured by Fdez-Gubieda *et al.* (2013) that a disordered ferric phosphate-like phase forms at the beginning of the time-course, which is quickly ( $< 30$  m) converted into magnetite. Very recently, Wen *et al.* (2019) reported electron diffraction evidence of very small crystals of  $\epsilon$ -Fe<sub>2</sub>O<sub>3</sub> in the very early stages of their time course study of MSR-1. The lack of consistency in this aspect of the biomineralization is, at least in part, due to the use of different analytical methods, each with a specific sampling depth, spatial resolution, chemical sensitivity, and structural sensitivity.

Marcano *et al.* (2017) recently reported results from a time-course experiment which showed that the cell growth phase (lag vs. exponential vs. stationary) at the time of Fe-induction had an influence on the magnetite biomineralization process in *M. gryphiswaldense* strain MSR-1. They showed that magnetosome particle synthesis is initially slow but eventually leads to the production of larger particles and a higher cellular magnetite content for iron-depleted cultures where cells are in the exponential phase at the time of iron-induction, compared to those in the arrested growth state. This dependence on specific experimental conditions could explain the apparent lack of consistency in the results from previous time course studies.

Although numerous efforts have been made to reveal the mechanism of magnetosome biomineralization inside MTB cells, several critical questions still need to be addressed: *Are there mineral (other than magnetite) precursors formed before magnetite magnetosome formation? If they exist, can we identify and locate these precursors? How are different precursor species and/or Fe ions inside magnetosome vesicles converted to magnetite, Fe<sub>3</sub>O<sub>4</sub>? How do they become organized into chains with aligned magnetic moments?*

One approach to address these issues is to use spatially resolved methods to characterize the chemical and magnetic properties of MTB on an individual cell and individual particle basis throughout the process of biomineralization. Here we report results of a time course study of the biomineralization of magnetite magnetosomes in *Magnetospirillum magneticum* strain AMB-1. We used X-ray absorption spectroscopy (XAS) and XMCD measured at the Fe L<sub>3</sub>-edge by

scanning transmission X-ray microscopy (STXM) to characterize cellular interior and individual magnetosomes in cells at various time points after initiation of biomineralization. XAS can identify different Fe species and thus identify precursor particles and possibly soluble Fe species (Zhu *et al.* 2016). XAS and XMCD can be used to monitor how the ratio of Fe(II) to Fe(III) changes as the biomineralization of Fe<sub>3</sub>O<sub>4</sub> proceeds. The power of our approach over most earlier time course studies is the ability to examine and spectroscopically analyze individual particles within a single cell. Our strategy was to start with cells grown in the absence of Fe which do not contain magnetosomes, and then to initiate magnetosome biomineralization by inoculating these cells into standard Fe-containing culture medium. We then sampled at various times during a 48 h period after the start of the time course, and subsequently measured TEM and STXM from those samples in order to investigate magnetosome biomineralization and chain formation over time.

## 2. Experimental

### 2.1 Sample preparation

Cells of *M. magneticum* strain AMB-1 were initially grown in a Fe-rich liquid medium under controlled microaerobic conditions with 1.5% O<sub>2</sub> in the headspace of the culture, as previously described (Le Nagard *et al.* 2018). The growth medium contained, per liter: 1.0 mL modified Wolfe's mineral elixir (Wolin *et al.*, 1963, Bazylinski *et al.*, 2000), 0.1 g KH<sub>2</sub>PO<sub>4</sub>, 0.15 g MgSO<sub>4</sub>·7H<sub>2</sub>O, 2.38 g (4-(2-hydroxyethyl)-1-piperazineethanesulfonic acid (HEPES buffer), 0.34 g NaNO<sub>3</sub>, 0.1 g yeast extract (BD 210929), 3.0 g Becton Dickinson (BD) Bacto™ Soytone (BD 243620), 4.35 mL potassium lactate (60% solution) and 5 mL Fe (III) citrate 10 mM stock solution.

Several weeks prior to starting a time course experiment, cells were grown in a Fe-depleted liquid growth medium similar to the Fe-rich growth medium except that the amount of BD Bacto™ Soytone was reduced to 1.0 g/L and the Fe(III) citrate and mineral solutions and the yeast extract were omitted. For the first set of samples (batch A, November 2017), cells were



grown in the Fe-depleted medium with 5% O<sub>2</sub> in the headspace. The increased O<sub>2</sub> concentration led to a quicker decrease in the number of magnetosomes per cell compared to cultures grown in Fe-depleted conditions with 1.5% O<sub>2</sub> in the headspace. It took 5 successive inoculations into fresh, Fe-depleted medium over a 2-week period to achieve cultures in which standard measures of a magnetic population – hanging drop and reflectivity modulation over a magnetic stirrer – indicated that most cells had lost their magnetism. In addition, transmission electron microscopy (TEM) showed most cells did not contain particles, although some had 1 or 2 particles. For batch B, the O<sub>2</sub> concentration in the headspace was increased to 20%, which caused cells in the culture to grow more vigorously, and to become non-magnetic even more quickly than at 5% O<sub>2</sub>. Respectively, >10 and 7 stages of depletion were performed for the batch A and B samples. At each stage, 1 mL of the (n-1) stage culture was inoculated into 60 mL of fresh Fe-depleted medium and incubated at 32 °C for 3-4 days in order to reach the stationary phase, before performing the next transfer. The magnetism of the culture was assessed at each stage using the hanging drop test, in which the response of the cells to an external magnetic field is studied using optical microscopy (Le Nagard *et al.*, 2018b). TEM was also used to estimate the number of particles per cell. For both batch A and batch B, there was no observable change in the hanging drop test and in TEM analysis results after 5-6 depletion stages.

The time course experiment was initiated by inoculating 30 mL of the Fe-depleted culture into 30 mL of the Fe-rich medium under anaerobic conditions. O<sub>2</sub> was immediately added to the culture after inoculation to obtain a concentration of 1.5% O<sub>2</sub> in the headspace of the culture. Samples were then removed from the culture at intervals of 0, 10, and 30 min (m) and 1, 2, 4, 5.7, 8, 12, 24, and 48 hours (h). Immediately after collecting a culture sample, the extracted aliquot was placed into a centrifuge vial and heated at 60 °C for 10 m to kill the cells and stop magnetosome biomineralization (Cazares *et al.* 2015). These samples were then stored at 4 °C until they were prepared for TEM and STXM.

For the batch A samples, ~2 µl were drop cast on to formvar coated 3 mm TEM grids. A washing step was not applied, and as a consequence, most of the cells were encrusted with

residual salts from the culture medium. For the batch B samples, 3 different sample mounting approaches were used. Immediately after heat sterilizing the cells at each time point during the time course, about 2  $\mu$ l were drop cast on to C-flat 3 mm TEM grids (<https://www.protochips.com/products/c-flat/>). After investigation by TEM it was found that there were still some residual salts (but much less than in the batch A samples) so a new set of batch B samples for STXM was prepared using glutaraldehyde fixation (Chao & Zhang 2011) followed by multiple washings in distilled deionized water and centrifuge separations. This has been shown to result in samples free of salt precipitates, with cells retaining the particles in their as-grown state (Le Nagard *et al* 2018a). The glutaraldehyde-fixed material was drop cast on silicon nitride windows (Norcada) and formvar coated TEM grids.

## 2.2 Scanning Transmission X-ray microscopy (STXM)

STXM analyses were performed at HERMES, the soft X-ray spectromicroscopy beamline at SOLEIL (St. Aubin, France) (Belkhou *et al*, 2015, Swaraj *et al.*, 2017). STXM methodology has been described in detail previously (Hitchcock 2012, Hitchcock 2015). Briefly, monochromated X-rays are focused to a  $\sim$ 30 nm spot by a Fresnel zone plate. The sample is positioned at the focal point and x-y raster scanned while recording the intensity of the transmitted X-rays. After locating cells of interest, aided by optical imaging and, in some cases, TEM, STXM images were measured at a sequence of photon energies (a stack). In all cases, the region measured contained a suitable area free of cells to measure the incident flux ( $I_0$ ), which is needed to convert transmitted intensities to optical density (OD). Circular right (CR) polarized light was used without any applied magnetic field. For some samples measurements were performed with both helicities – i.e. both circular left (CR) and circular right (CL) polarized light. XMCD maps were then generated from the difference of OD-converted CR- and CL-images at 708.2 eV - the energy of strongest X-ray magnetic circular dichroism (XMCD) signal for magnetite (Goering *et al.* 2007, Zhu *et al.* 2015). XMCD spectra are the (CR – CL) difference, recorded at all energies across the Fe  $L_3$  edge. STXM studies of the batch A samples were performed in November 2017 with the sample tilted at 32° relative to the focal plane. For the batch B samples, XAS and

XMCD were measured in December 2018, using both 0° tilt (X-ray beam direction normal to the sample plane) and 30° tilt (sample grid tilted at 30° relative to the focal plane).

### 2.3 Data analysis – STXM, XAS & XMCD

Most of the results were obtained using XAS stacks - a set of images measured over a sequence of photon energies in the Fe L<sub>3</sub> region (700 – 717 eV). After image alignment and conversion of the transmission signal to OD, the many-energy stacks were further processed by extracting internal reference spectra from unique morphologies such as the particles and the cytoplasm, then fitting the stack to those reference spectra in order to generate component maps. In some cases, the component maps are presented as color coded composites in which the signal of each component is scaled to fill its color scale (so called rescaled, rather than absolute color composites) (Hitchcock, 2012). In cases where both CR and CL multi-energy stacks were acquired, these were combined into a single file prior to alignment and OD conversion, and then separated to allow generation of XMCD stacks from the difference (CR-CL) which allowed extraction of the magnetic signal from individual particles. All STXM data analysis was performed using aXis2000 (<http://unicorn.mcmaster.ca/aXis2000.html>).

In this work, in contrast to typical XMCD measurements in materials science, the intrinsic magnetic properties of a sample are measured without using any applied magnetic field. There are strict geometric requirements to measure magnetization by XMCD. As outlined in **Fig. 1**, the magnitude of the XMCD signal is determined by the dot product of the magnetization vector of the sample and the polarization vector of the photon. The polarization vector of circularly polarized photons points either forward (CR) or backward (CL) along the X-ray propagation direction. In order to have a measurable XMCD signal there must be a non-zero projection of the magnetization vector of the sample along the photon polarization. The magnetization vector of chains of magnetosomes in magnetotactic bacteria grown in high-Fe culture is typically along the cell axis. Thus, a cell lying flat on its support should be positioned such that the long axis of the cell is horizontal and the sample is tilted out of the plane normal to the X-ray propagation direction. We typically use a polar tilt angle of ~30° for which the projection of an in-plane,

horizontally oriented magnetic moment is 50%. Since monitoring the development of the chains and their magnetic alignment is the goal of this project, we have made measurements at both  $0^\circ$  and  $30^\circ$  tilt angles. Any XMCD signal detected with the sample at a tilt angle of  $0^\circ$  indicates there is an out-of plane component to the magnetization (i.e. a component orthogonal to the grid on which the cell is deposited).

#### *2.4 Data analysis –particle size distributions from statistical evaluation of TEM images*

The average number of particles and their typical size in cells of the glutaraldehyde-fixed Batch B samples were determined by TEM. Individual cells were randomly selected on the grids and imaged at 40,000x – 60,000x magnification. This study was performed after the STXM measurements, to avoid damaging the samples with high magnification TEM. 20 cells were imaged per sample, and a minimum of N=18 cells in each sample were subjected to detailed image analysis. Particles were counted and measured manually. Large variations in the contrast of the particles (size dependency and inhomogeneous background) made it difficult to use an automated procedure. The oval selection tool of the ImageJ software was used to draw a shape that best matched the projection of each particle in the focal plane. The surface area of that projection was measured and converted to a diameter, assuming the particles to be spherical. There is significant uncertainty in the measurement of particles smaller than 10 nm, due to insufficient spatial resolution at the magnifications used in this study. These particles were excluded from the final results. After excluding these very small particles, independent analyses of the 24 h sample performed by two different experimentalists differed in the average number and size of particles by only 7% and 2% respectively.

### **3. Results**

#### *3.1 Overview of the time course samples*

**Figure 2a** shows STXM maps of the Fe-containing particles in one cell from each time course point for the batch B samples. Early in the time course (10 m, 30 m), cells contained no or

just a few particles. The average Fe L<sub>3</sub> spectrum of all the particles within each cell in **Fig. 2a** are plotted in **Fig. 2b**. Over the time course there is a general increase in the intensity of the Fe L<sub>3</sub> signal, and some shape changes, which are discussed in a later section. A detailed description of the particle size and number per cell at each time point in the batch B time course, as measured by TEM is presented in section 3.2. In terms of particle numbers, there were no significant differences between the samples taken at 10 m and 30 m after the start of the experiment, followed by an increase in the number of particles per cell in subsequent time points. Cells from the 1 h and 2 h sample exhibited only a few particles. A transition occurred in cells of the 4 h and 5.7 h samples, in which many more particles were present and chains started to appear. Cells in samples taken at later times contained relatively large magnetite particles assembled in chains of varying lengths. The average number of particles per cell and extent of chain formation at 48 h were indistinguishable from stationary phase cells grown in Fe-rich media.

**Supplemental figure S-1** shows STXM images of cells from **batch A** at each time point. In the batch A experiments, particles appeared after 2 h in some cells. XAS spectra at the Fe L<sub>3</sub> edge of particles from these experiments are presented in **Supplemental Fig. S-1g**. A systematic increase in the X-ray absorption at ~710 eV of individual particles with time was observed. The images and STXM-XAS results showed that a mixture of large and small particles was present in cells from the 4 h sample. Only a few isolated particles were observed in the <2 h samples. By 48 h, STXM images of the cells examined were indistinguishable from STXM images of stationary phase AMB-1 cells cultured in Fe-rich medium, both in terms of imaging (**Fig. S-1f**), and Fe L<sub>3</sub> spectra (**Fig. S-1g**). On a qualitative basis, the trends seen in batch A and B are similar.

### *3.2 Statistics of particle size and number of particles per cell*

A stacked bar chart of the size distribution of particles per cell at each time point, as determined by TEM, is shown in **Figure 3a**. The change over the time course in numbers within each of 4 particle size ranges is presented on a log(time) plot in **Fig. 3b**. The numerical data is

presented in **Supplemental Table S-2** while **Fig. S-2** shows histograms of the size distribution at each time point. Fig. 3b indicates there is a 30 min lag phase followed by growth of particles. This is consistent with recent results on AMB-1 reported by Amor *et al.* (2018, 2019) in which they find evidence for a similar lag phase, which they suggest correlates with the build-up of a pool of intracellular iron, distinct from the magnetosomes. The average number of particles per cell was about 13 after 2 h. Many of these particles were very small, probably below the spatial resolution of STXM. Particle counts per cell for AMB-1 cells grown in an Fe-rich medium reported in the literature range from 11 (Wang *et al.* 2013) to 20 (Tanaka *et al.* 2008).

### 3.3 Reference STXM – XAS/XMCD of mature AMB-1 magnetosomes

**Figure 4** presents a STXM image of a AMB-1 cell taken from stationary phase culture grown in Fe-rich media, along with magnet maps, and the XAS and XMCD spectra of the magnetosomes. The sample was tilted at 30° relative to the X-ray propagation direction and CR was used. **Figure 4a** is the average of 36 OD images from 704 to 717 eV while **Fig. 4b** is a color coded composite of component maps derived by fitting the Fe L<sub>3</sub> stack to the spectra presented in **Fig. 4c**. The fitting identifies the magnetosomes with a parallel (red) and those with an antiparallel (blue) alignment of their magnetic moment with respect to the circular polarization vector of the photon (see **Fig. 1**). In **Fig. 4c** the dots are the average spectra of all the magnetosomes with parallel (red) or anti-parallel (blue) magnetic alignment, while the solid lines are spectra reported for synthetic magnetite (Goering *et al.* 2007) with their intensity scale adjusted to match the OD of the AMB-1 magnetosome spectra. Although there is an offset, the min-max magnitude of the XMCD signal in the AMB-1 magnetosomes is the same as that in magnetically-saturated magnetite, indicating the magnetization of the magnetosomes is fully saturated and the magnetic moment is oriented in the plane of the sample. A similar approach was used to demonstrate that the magnetism of magnetosome in cells of *Magnetovibrio blakemorei* strain MV1 is saturated (Kalirai *et al.* 2016). We note that normally CR and CL spectra are normalized to the edge jump and presented as an asymmetry ratio. However, there

was not sufficient beam time to allow measurement of full Fe L<sub>23</sub> spectra for this type of normalization.

**Figure S-3** presents results from XAS-XMCD studies of two AMB-1 cells from the 48 h time point in batch B, measured using CR with the sample tilted 30° relative to the X-ray beam. In this case, in contrast to Fig. 4, the magnetic polarity of each magnetosome in an individual cell is the same, but the magnetic moment of the chains in the left cell are pointing opposite to that in the right cell, as shown by the color coded composite of signals from an XMCD stack map (**Fig S-3a**). Full Fe L<sub>3</sub> stacks of the left cell were recorded using both CR and CL polarization, in order to obtain the XAS and XMCD signals. **Fig. S-3b** compares the spectra of magnetosome particles from the 48 h sample recorded with both circular polarizations, in comparison to the data from **Fig. 4** and that of magnetite (Goering *et al.* 2007). The spectrum of the cytoplasm (also plotted in **Fig. S-3b**) does not have any Fe L<sub>3</sub> signal. The CR stack was fit to the parallel and anti-parallel reference spectra to generate component maps, which are presented as a color-coded composite in **Fig. S-3c**. Within each color the signal for that component has been rescaled to the full 0-255 scale. At the particles the parallel signal is strong while the anti-parallel signal is weak, possibly just noise. The XMCD signal (**Fig. S-3b**) is strong, similar in intensity to that of an AMB-1 cell taken from stationary phase culture grown in Fe-rich media (**Fig. 4**), and to that of XMCD of magnetically saturated magnetite (Goering *et al.* 2007), scaled \*0.5 to account for the experimental geometry (tilt angle of 30°).

### 3.4 Time-dependent STXM-XAS Study of the Biomineralization Process

Typically, 2 or 3 cells at each time point of the batch B time course were measured in detail. In each case, there were only a few scattered individual particles present in cells up to 1 h. Disordered chains and larger particles appear in cells from the 2 h sample. Well-developed chains similar to those in cells from stationary phase culture grown in Fe-rich medium were observed in cells from the 24 h and 48 h samples (see **Fig. 2a**). Cells from the 8 h time point of batch A, and the 5.7 h and 24 h time points of batch B were particularly interesting and are highlighted in the next sections.

A detailed analysis of a cell from the 8 h sample in batch A is presented in **Fig. 5**. **Figure 5a** shows that this cell contained one chain with 6 particles (left chain, red), a second chain in the middle with 3 small particles (middle chain, cyan) which is interpreted as a “growing” chain, and a third chain at the right with 3 very small particles which are interpreted as particles in the early stages of growth (precursor, green). In addition, there is a single large magnetosome (blue). **Figure 5b** compares the background subtracted Fe L<sub>3</sub> spectra of the large magnetosome, the left chain, the middle (“growing”) chain and the chain of precursor particles from this cell, on an absolute OD scale. **Fig. 5c** plots the same spectra on a constant intensity format, with comparisons to reference spectra of FeCl<sub>3</sub> (Nagasaka, *et al.* 2013) and parallel and antiparallel circular dichroic spectra of synthetic magnetite (Goering *et al.* 2007). The spectrum of the large magnetosome is similar to that of magnetite with antiparallel magnetic moment orientation relative to the CR light. The spectrum of the left chain is similar to that of magnetite with parallel magnetic moment orientation relative to the CR light. In the spectrum of the particles in the middle chain (cyan) the signal at 708.4 eV is significantly more intense than that of magnetite. This is consistent with  $\alpha$ -hematite (Zhu *et al.* 2015). **Supplemental figure S-4** plots the Fe L<sub>3</sub> spectra of several of the particles from early time course samples in comparison with the spectra of  $\alpha$ -hematite (Zhu *et al.* 2015), ferrihydrite (Joshi *et al.* 2018), FeCl<sub>3</sub> (Nagasaka, *et al.* 2013) and Fe(III) phosphate (Miot *et al.* 2009). While the differences are subtle, in the spectrum of the particles of the 5h 40 m sample, the position and, especially, the intensity of the 708.4 eV signal relative to the main peak at 709.8 eV is close to that of  $\alpha$ -hematite. However the spectrum of the particles in the precursor chain of the 8 h sample is more similar to the Fe L<sub>3</sub> spectra of ferrihydrite (Joshi *et al.* 2018) or FeCL<sub>3</sub> (Nagasaka, *et al.* 2013). The spectrum of the particles in the “growing” chain is intermediate between the two, although closer to the spectrum of magnetite.

To further focus on results from specific time course points, the STXM-XMCD results from cells taken at the 5.7 h (5 h 40 m) and 24 h time points are discussed below. In addition, results and discussion of the 4 h sample from batch B is given in the Supplemental Information. **Figure**



6 presents results from the 5.7 h sample (batch B) measured with the sample tilted at both  $0^\circ$  and  $30^\circ$  relative to the X-ray beam. In this case the cell examined was drop cast directly from the 5.7 h solution onto a C-flat grid, without washing. Despite that, the cell was very clean, without adhering salts from the culture. **Fig. 6a** and **6b** present TEM images of the same cell, measured after the STXM measurements. There are clear signs of carbon deposition in the rectangle irradiated during the measurement (**Fig. 6a**). **Figure 6c** shows the sum of all images in an Fe  $L_3$  stack map, measured with the sample normal to the beam (tilt =  $0^\circ$ ). **Figure 6d** represents an XMCD map at 708.2 eV measured at tilt =  $0^\circ$  showing that a number of the particles exhibit out-of-plane magnetization. **Figure 6e** shows an XMCD map of the same set of particles, measured at tilt =  $30^\circ$ . The XMCD signal intensity has significantly increased and all but the two particles at the ends of the disorganized chain have the same magnetic moment direction, while the magnetic moment of the particles at the end is in the opposite direction. The magnitude of the XMCD signal of the leftmost particle is of opposite sign and twice as strong at  $0^\circ$  (-0.08) than at  $30^\circ$  tilt (+0.04). **Figure 6f** presents XAS measured with CR and CL polarization and the resulting XMCD spectrum, averaged over all the particles in **Fig. 6e** which have a negative XMCD signal (dark). A clear XMCD signal was obtained for this cell and the positioning of the particles was such that chain formation appears to be occurring (**Fig. 6e**).

**Figure 7** plots the Fe  $L_3$  spectra of five different iron-containing regions of an AMB-1 cell from the 24 h time point (batch B). Spectral variability in the Fe  $L_3$  stack was assessed by careful examination of the Fe  $L_3$  spectra of the different morphologies. Five distinct Fe  $L_3$  spectra were detected, which when used to fit the stack, resulted in a high quality fit with very small residuals and clear, spatially localized component maps. A multivariate statistical analysis using the PCA\_GUI code (Lerotic *et al.*, 2005) supported the existence of 6 or 7 independent components, consistent with the analysis presented here. These spectra were used to derive the results presented in **Fig. 8**, which includes component maps from the 5-component fit to the Fe  $L_3$  stack, and a color coded composite map for cells of the 24 h sample (glutaraldehyde fixed). **Fig. 8a** shows an OD-converted image of the full cell. **Fig. 8b** shows the average of all images in a

60-energy Fe L<sub>3</sub> stack measured on the right part of the cell, which has well-developed magnetosome chains. The component maps, i.e., maps of the areas with spectra like one of the 5 reference spectra, are displayed in **Fig. 8c-g**. A color coded composite of the parallel XMCD (red), cytoplasm (green) and antiparallel XMCD (blue) maps is presented in **Fig. 8h**. A notable feature of this cell is a well-defined ‘ring’ or rim around the central, expanded part of the cell. While the spectrum of the rim has a large non-Fe component, it also has a broad Fe L<sub>3</sub> signal which is at higher energy than the Fe signal of the weak but statistically significant Fe L<sub>3</sub> signal in the cytoplasm of the cell. Finally, one of the particles has a strong Fe(III) signal, different from the small particles in the 5.7 h and 8 h cells which show enhanced 708.4 eV signal. That Fe(III) particle did not exhibit any XMCD (compare **Fig. 8d** and **Fig. 8e, 8f**).

**Fig. 9** presents the circular dichroic dependent Fe L<sub>3</sub> XAS spectra and the derived XMCD signal from the 10 magnetosomes in the 24 h cell (**Fig. 8e**). The intensity scale is that for the optical density of the AMB-1 24 h cell data. **Fig. 9** also presents the parallel and antiparallel spectra of magnetite reported by Goering *et al.* 2007, scaled to match the magnitude of the signal from the AMB-1 cell. After correcting by a factor of 2 for the projection of the 30° tilted sample onto the spin vector of the X-rays, the magnitudes of the XMCD signal of pure magnetite and that of the magnetosomes are very similar. This indicates that, after 24 h of the time course, the particles are magnetite and their magnetization is fully saturated.

**Supplemental Figure S-6** compares color-coded composites of the Fe-rich components obtained from two different models for mapping the chemical components of the 24 h time point sample from batch B from the Fe L<sub>3</sub> stack. **Fig. S-6a** was obtained from the stack measured with CL using only 4 components (spectra of regions with XMCD+, XMCD-, cytoplasm and Fe(III), without an explicit ‘rim’ signal) while **Fig. S-6b** was obtained from the stack measured with CR using the 5 components displayed in **Fig. 7**. If a specific spectrum of the ‘rim’ is not included then the area corresponding to the ‘rim’ is fit with the nominal CL component. However, if the ‘rim’ spectrum is included in the fit then the rim signal fits to both the rim and regions in the

vicinity of the magnetosomes. The model including an explicit rim spectrum is better.

**Supplemental Figure S-7a-c** are images of the XMCD stack for the 24 h sample. **Figure S-7d** displays the XMCD spectra of the magnetosomes while **Fig. S-7e** presents the XAS spectrum of the rim. The XMCD spectrum of the 'rim', plotted in **Fig. S-7d**, showing there is no detectable XMCD in the 'rim' region.

## 4. Discussion

### 4.1 What we have learnt?

Our results clearly show that small numbers of iron oxide particles were generated in cells of *M. magneticum* strain AMB-1 grown without a major source of iron, relatively early (<30 m) after the major source of iron, Fe(III) citrate, was introduced. These particles were significantly smaller than those in magnetosomes in cells of cultures incubated for longer periods. The spectra of the particles in cells taken at 10 m, 30 m, 1 h, and 2 h showed a signal at 708.4 eV that is stronger than that of magnetite, indicating contributions from an Fe(III)-rich precursor. The samples on TEM grids or SiN<sub>x</sub> windows were stored under dry N<sub>2</sub> from the time of preparation to studies at SOLEIL. It has also been shown that magnetosome magnetite crystals which are surrounded by their lipid membrane oxidize very slowly even when exposed to air for many months (Zhu *et al.* 2015). Thus we conclude that the additional oxidized character of the smaller particles in the early time points is a characteristic of the biomineralization of magnetite in *M. magneticum*, and thus those particles can be considered precursors to magnetite. XMCD maps (CR and CL at 708.2 eV, the energy of strongest XMCD contrast) and/or Fe L<sub>3</sub> stacks were measured for 5 of the 9 samples.

One concern in interpreting these results is the question of the degree to which particles observed at early time points might have been magnetite magnetosomes in cells inherited from the original inoculum (which was grown in Fe-rich medium) or possibly even iron oxide particles grown in Fe-depleted medium due to the presence of the very low concentration of Fe required for cell growth, possibly present in Bacto<sup>TM</sup> Soytone. The 10 m samples in both batch A

and B contained a few cells with one particle that was quite large (40-50 nm) suggesting that it could be a residual magnetosome from the original pre-Fe-depletion culture, despite many cycles of re-inoculating in Fe-depleted medium to dilute the original cells and reduce the number of magnetosomes per cell by allowing the cells to divide a significant number of times. Due to this ambiguity we have placed greater reliance on samples at later time points ( $\geq 1$  h) in developing our interpretation of these results.

In cells from the 4 h sample from batch B, 1 out of 5 particles showed an XMCD signal with the sample at  $0^\circ$  tilt. (**Fig. S-5**). The 4 small particles in the same cell did not exhibit a measurable XMCD signal. Magnetosome crystals in cells grown for many generations in Fe-rich growth medium only exhibit XMCD if the cell is  $\sim$ horizontal and tilted at  $30^\circ$  to the beam propagation direction (Lam *et al.* 2010). The observation of a strong out-of-plane magnetization is evidence that the magnetic particle was recently biomineralized. In the absence of chain formation and presumably magnetic dipolar interaction with adjacent magnetite particles, the magnetic moment could point in any direction. If the particle-particle magnetic interaction between pre-existing magnetosome(s) and a newly biomineralized magnetosome(s) is not strong enough to align the magnetic vector of the new one, the magnetic orientation of the newly forming magnetosome would be determined by external factors such as the local magnetic field of the earth at the time of particle formation. Winklhofer *et al.* (2007) reported that the degree of preferential alignment was 0.54:0.46 at a magnetic field of 0.26 G (about that of the earth in Hamilton, ON where the time course samples were grown) and rose only to 0.58:0.42 at a field of 0.50 G.

It should be noted that the visual gap between magnetosomes with opposite magnetic polarities (e.g. **Fig. 6e**) might not represent the real distance between these magnetosomes, since 2D projection images can mask the actual 3D distance information. In this regard, XMCD tomography, which can map the magnetization strength and direction of individual particles in 3D, of a cell displaying both in-plane and out-of-plane magnetization might provide additional insight into how MTB achieve the well organized and well correlated magnetism of adjacent magnetosomes. Electron tomography was very useful in showing that lipid vesicles in which

magnetosomes are formed bud from the exterior cell membrane (Komeli *et al.* 2004). Cells from the 5.7 h batch B contained numerous particles (>12 /cell on average), the crystals in some of which exhibited XMCD at 0° with opposing moment orientations (**Fig. 6**). When the same sample was measured at 30°, an XMCD signal was observed for the majority of the particles, indicating a chain with a more organized magnetic structure was being formed. In cells from the 24 and 48 h samples, the XAS spectra measured at 30° and the magnitude of the derived XMCD signal of the magnetosomes was similar to that of synthetic magnetite (Goering *et al.* 2007) (**Fig. S-3b**).

Iron oxide particles were observed in cells from the 1 – 8 h time points which had a measurably smaller diameter and weaker Fe L<sub>3</sub> signal than that of mature particles found in AMB-1 cells, and typically a stronger signal at 708.4 eV than is expected for magnetite. These particles are interpreted as growing particles and thus their properties are providing direct information about the biomineralization mechanism. The stronger 708.4 eV signal is evidence for a higher Fe(III) character than that of magnetite. The comparison of the position and intensity of the 708.4 eV signal relative to the main 709.8 eV peak with that in other Fe(III) compounds (**Fig. S-4**), suggests that  $\alpha$ -hematite (Zhu *et al.* 2015) is a possible intermediate in the development of mature magnetosomes. We note that  $\alpha$ -hematite was also found in previous time course studies by Baumgartner *et al.* (2013) and Firlar *et al.* (2016, 2019), although both of those studies, along with that by Fdez-Gubieda *et al.* (2013), concluded that a phosphate-rich ferric hydroxide phase was involved. We also find a precursor signal consistent with FeCl<sub>3</sub> and/or ferrihydrite, in agreement with the main conclusions of Baumgartner *et al.* (2013) and Fdez-Gubieda *et al.* (2013). A better understanding of the role of these two species in the biomineralization pathway is now required. We note that the statistical quality of the Fe L<sub>3</sub> spectra from the particles in the earlier time points is limited. In addition the spectra are averaged over several particles, which may be at different stages of development and thus might have different speciation. Finally, we did not have enough beam time to adequately sample times below 1 hour and thus our results are silent in that early period, where Wen *et al.* (2019) find evidence for  $\epsilon$ -Fe<sub>2</sub>O<sub>3</sub> from single particle electron diffraction.

A striking observation in this study is that small particles are formed at multiple places in the cell, not necessarily in chains, and with seemingly no detectable ferromagnetism, or with randomly oriented magnetic moments. The observation of these putative precursor particles in

different cell locations and at different times time course points suggests that magnetosomes are not biomineralized simultaneously. Regarding the appearance of precursors at multiple sites within the cell, Scheffel *et al.* (2006) have shown that magnetite biomineralization is initiated at multiple discrete sites throughout the length of *Magnetospirillum* cells. Thus mature magnetosomes and magnetosome precursors can coexist in the same cell since some may grow faster than others. The acidic protein MamJ was shown to be responsible for anchoring the magnetosome to a filamentous structure now recognized as the protein MamK (Arakaki *et al.* 2008). As for the lack of ferromagnetism observed in these precursors, this could be because these small particles are not (yet) magnetite and thus not magnetic at room temperature. Alternatively they could be smaller than the ~30 nm super-paramagnetic limit in magnetite (Dunlop 1973), and thus subject to thermally induced re-orientation of their magnetic moment. A third explanation could be that the early particles are Fe-rich polyphosphates formed in the cytoplasm, as was found in some other bacterial systems (Miot *et al.* 2009). STXM measurements at the P 2p or P 1s edge could be used to investigate this last possibility.

In the intermediate time points (4 – 8 h) chain formation is increasingly seen, and a larger fraction of the particles are located in chains with an in-plane magnetic moment (e.g. the 5.7 h batch B sample, **Fig. 6**, and the 8 h batch A sample, **Fig. 5**). It is only in the 24 h and 48 h samples that the size, spectroscopy, magnetic moment magnitude and orientation match that of magnetosome chains in mature AMB-1 cells grown in Fe-rich culture.

From a microbiological point of view, this study shows that *M. magneticum* strain AMB-1 will grow for extended periods of time when several nutrient sources usually added to the growth medium are omitted or added in significantly lower concentration – in this case, yeast extract, Bacto™ Soytone, mineral solution in addition to Fe(III) citrate, the major Fe source of the normal growth medium. Increasing the O<sub>2</sub> concentration does not prevent growth either, showing that *M. magneticum* can adapt to a relatively wide range of conditions, from microaerobic to fully oxic conditions. When cultured at high concentrations of O<sub>2</sub> and low concentrations of Fe for extended periods of time, the cells biomineralize only a few crystals and grow as vigorously as in normal media. These findings raise important questions regarding the magneto-aerotaxis model for the function of magnetosomes in magnetotactic bacteria, at least for *M. magneticum*. If

the cells grow in presence of high concentrations of O<sub>2</sub> expending energy to produce magnetosomes no longer seems advantageous if their only role is to help the cells locate the OAI more efficiently. Finally, as seen during this and other time course experiments, cells start biomineralizing new crystals quite quickly once placed under low O<sub>2</sub> and relatively high Fe concentrations. This shows that the machinery used to perform biomineralization is conserved during periods of Fe starvation and that it is quickly reactivated when the environmental conditions are suitable.

#### 4.2 Suggestions for future studies

While these results contribute to our understanding of magnetosome biomineralization, they are still ambiguous with regard to the identity of the Fe(III)-rich precursor species. Many studies have shown that it is possible to use XAS and XMCD to differentiate among the candidate species ( $\alpha$ -hematite, Fe phosphates, ferrihydrite). However better statistics than we were able to achieve in this study are required. In part this is a function of limited experimental time at the synchrotron STXM, and in part a consequence of limited spatial resolution. The former issue can be addressed by focusing on just a few representative cells in the 1-6 h time course points where the evolution of the chemistry and organization is occurring. More precise spectra could then be fit to a linear combination of the 2 contributions and used to extract the ratio of the precursor and magnetite components as a function of time. Higher spatial resolution can be achieved by using the emerging method of soft X-ray ptychography (Thibault *et al.* 2014, Hitchcock 2015) which has already been applied to MV-1 MTB (Zhu *et al.* 2016). In addition to XAS and XMCD in 2D projection, it would be beneficial to perform XMCD tomography in order to locate the spatial orientation of the magnetic moment of particles in cells like the 5.7 h sample (**Fig. 6**).

## 5. Summary

This work has presented results of a time course study of an intracellular biomineralization process elaborating the formation of mature magnetite magnetosomes in cells of the

magnetotactic bacterium *M. magneticum* strain AMB-1. Our results indicate that the initially-produced particles are Fe(III)-rich. Later, some of the Fe(III) is reduced to form magnetite. The particles in the growth phase are primarily disorganized but start forming organized chains at about 4 h of growth and reach a mature stage between 24 to 48 h, with number per cell and size of the magnetosomes similar to that observed in cells at saturation phase grown in Fe-rich culture. Our results are consistent with most previous studies which report the presence of some type of excess Fe(III) during early growth. However, few of these studies resulted in the identification of a specific Fe(III)-rich species. Our Fe L<sub>3</sub> XAS results suggest  $\alpha$ -hematite is a precursor to magnetite in AMB-1, but do not exclude other possible precursors such as ferrihydrite. Future studies will reveal whether these two species contribute to the same or to distinct pathways towards magnetite. In addition, this work provides additional insight into the magnetite biomineralization mechanism through detailed Fe L<sub>3</sub> XAS and XMCD spectra of precursors and immature magnetosomes.

**Acknowledgements:** This work was supported by NSERC (Canada) (Hitchcock) and by the U.S. National Science Foundation grant EAR-1423939 (Bazylinski). The measurements were carried out at the STXM on the Hermes beamline at Synchrotron SOLEIL. We thank Marcia Reid for excellent assistance with TEM viewing and preparation of the gluteraldehyde fixed samples.

## References

- Arakaki, A., Nakazawa, H., Nemoto, M., Mori, T., Matsunaga, T. (2008) Formation of magnetite by bacteria and its application, *J. R. Soc., Interface*, 5, 977–999.
- Amor, M., Busigny, V., Louvat, P., Tharaud, M., Gélbert, A., Cartigny, P., Carlut, J., Isambert, A., Durand-Dubief, M.I., Ona-Nguema, G., Alphandery, E., Chebbid, I., Guyot, F. (2018) Iron uptake and magnetite biomineralization in the magnetotactic bacterium *Magnetospirillum magneticum* strain AMB-1: an iron isotope study. *Geochem. Cosmochim. Acta* 232, 225–243
- Amor, M., Tharaud, M., Gélbert, Komeili, A., (2019) Single-cell determination of iron content in magnetotactic bacteria: implications for the iron biogeochemical cycle, *Environmental Microbiology*, XX, YYY-YYY. doi: 10.1111/1462-2920.14708



- Bazylinski, D.A. (1999) Synthesis of the bacterial magnetosome: the making of a magnetic personality  
International Microbiology, 2, 71-80
- Bazylinski, D.A., Dean, A.J., Schüler, D. Phillips, E.J.P., Lovley, D.R. (2000) N<sub>2</sub>-dependent growth and  
nitrogenase activity in the metal-metabolizing bacteria, geobacter and magnetospirillum species.  
Environmental Microbiology, 2, 266–273.
- Bazylinski, D.A., Frankel, R.B., Heywood, B.R., Mann, S., King, J.W., Donaghay, P.L., Hanson, A.K.,  
(1995) Controlled biomineralization of magnetite (Fe<sub>3</sub>O<sub>4</sub>) and greigite (Fe<sub>3</sub>S<sub>4</sub>) in a magnetotactic  
bacterium. Applied and Environmental Microbiology 61, 3232–3239.
- Baumgartner, J., Morin, G., Menguy, N. Gonzalez, T.P., Widdrat, M., Cosmidis, J., Faivre, D. (2013)  
Magnetotactic bacteria form magnetite from a phosphate-rich ferric hydroxide via nanometric ferric  
(oxyhydr)oxide intermediates, Proc. Nat. Acad. Sci. 110, 14883–14888.
- Belkhou, R., Stanesco, S., Swaraj, S., Besson, A., Ledoux, M., Hajlaoui, M. Dalle, D. (2015) HERMES: a  
soft X-ray beamline dedicated to X-ray microscopy, J. Synchrotron Radiation, 22(4): 968-979.
- Cazares. L.H., Van Tongeren, S.A., Costantino J., Kenny, T., Garza, N.L., Donnelly, G., Lane, D., Panchal,  
R.G., Bavari, S. (2015) Heat fixation inactivates viral and bacterial pathogens and is compatible with  
downstream MALDI mass spectrometry tissue imaging, B.M.C. Microbiology 15: 101 (1-11).
- Chen, A.P., Berounsky, V.M., Chan, M.K., Blackford, M.G., Cady, C., Moskowitz, B.M., Kraal, P.,  
Lima, E.A., Kopp, R.E., Lumpkin, G.R., Weiss, B.P., Hesse, P., Vella, N.G.F. (2014) Magnetic  
properties of uncultivated magnetotactic bacteria and their contribution to a stratified estuary iron cycle.  
Nature Communications, 5, 4797.
- Chen T., Wang, Z., Wu, X. Gao, X. Li, L., Zhan, Q.(2015) Magnetic properties of tidal flat sediments on  
the Yangtze coast, China: Early diagenetic alteration and implications, The Holocene 25, 832-843.
- Chao, Y, Zhang, T. (2011) Optimization of fixation methods for observation of bacterial cell morphology  
and surface ultrastructures by atomic force microscopy, Appl. Microbiol. Biotechnology 92, 381-392.
- Cosmidis, J., Benzerara, K., Morin, G., Busigny, V., Lebeau, O., Othmane, G., Dublet, G., Noel, V.  
(2014) Biomineralization of iron-phosphates in the water column of Lake Pavin (Massif Central, France),  
Geochimica et Cosmochimica Acta 126, 78-96.
- Dunlop, D.J. (1973) J. Superparamagnetic and Single-Domain Threshold Sizes in Magnetite, Geophysical  
Research 78, 1780-1793

- Faivre, D., Schuler, D. (2008). Magnetotactic Bacteria and Magnetosomes, Chem. Rev. 108, 4875-4898.
- Faivre, D., Böttger, L.H., Matzanke, B.F., Schüler, D. (2007) Intracellular Magnetite Biomineralization in Bacteria Proceeds by a Distinct Pathway Involving Membrane- Bound Ferritin and an Iron(II) Species, Angew. Chem., Int. Ed. Engl. 46, 8495-8499.
- Fdez-Gubieda, M.L., Muela, A., Alonso, J., García-Prieto, A., Olivi, L., Fernández-Pacheco, R., & Barandiarán, J. M. (2013) Magnetite biomineralization in *Magnetospirillum gryphiswaldense*: time-resolved magnetic and structural studies. ACS nano, 7(4), 3297-3305.
- Firlar, E., Perez-Gonzalez, T., Olszewska, A., Faivre, D., Prozorov, T., (2016) Following iron speciation in the early stages of magnetite magnetosome biomineralization, J. Mater. Res. 31, 547-555
- Firlar, E., Ouy, M., Bogdanowicz, A., Covnot, L., Song, B., Nadkarni, Y., Shahbazian-Yassar, R., Shokuhfar T. (2019) Investigation of the magnetosome biomineralization in magnetotactic bacteria using graphene liquid cell – transmission electron microscopy, Nanoscale 11, 698-705.
- Frankel, R. B., Papaefthymiou, G.C., Blakemore, R.P., O'Brien W. (1983) Fe<sub>3</sub>O<sub>4</sub> precipitation in magnetotactic bacteria, Biochim. Biophys. Acta 763, 147-159.
- Goering E., Lafkioti M., Gold S., Schuetz G.. (2007) Absorption Spectroscopy and XMCD at the Verwey Transition of Fe<sub>3</sub>O<sub>4</sub>, J. Magnetism and Magnetic Materials 310, e249–e251.
- HeyenU., Schüler D. (2003) Growth and magnetosome formation by microaerophilic *Magnetospirillum* strains in an oxygen-controlled fermentor, Appl. Microbiol. Biotechnol. 61, 536–544.
- Hitchcock, A.P. (2012) Soft X-ray Imaging and Spectromicroscopy, Chapter 22, Volume II of the *Handbook on Nanoscopy*, eds. Gustaaf Van Tendeloo, Dirk Van Dyck and Stephen J. Pennycook (Wiley) 745-791.
- Hitchcock, A.P., (2015) Soft X-ray spectromicroscopy and ptychography, J. Electron Spectroscopy and Related Phenomena 200, 49-63.
- Jogler, C. Schüler, D. (2007) in *Genetic Analysis of Magnetosome Biomineralization BT – Magnetoreception and Magnetosomes in Bacteria*, ed. D. Schüler, D., Springer Berlin Heidelberg, Berlin, Heidelberg, 133–161.
- Joshi, N., Filip, J. Coker, V.S., Sadhukhan, J., Safarik, I., Bagshaw, H., Lloyd, J.R. (2018) Microbial Reduction of Natural Fe(III) Minerals; Toward the Sustainable Production of Functional Magnetic Nanoparticles, Frontiers in Env. Sci. 6, 127.

- Kalirai, S.S., Lam, K.P., Bazylinski, D.A., Lins, U., A.P. Hitchcock, A.P. (2012) Examining the chemistry and magnetism of magnetotactic bacterium *Candidatus Magnetovibrio blakemorei* strain MV-1 using scanning transmission X-ray microscopy, *Chemical Geology* 300-301, 14-23.
- Komeili A, Vali H, Beveridge TJ, Newman DK (2004) Magnetosome vesicles are present before magnetite formation, and MamA is required for their activation *Proc Natl Acad Sci USA* 101, 3839–3844.
- Lam, K.P., Hitchcock, A.P. , Obst, M., Lawrence, J.R., Swerhone, G..D.W., Leppard, G..G., Tyliszczak, T. , Karunakaran, C., Wang, J., Kaznatcheev, K., Bazylinski, D., Lins, U. (2010) X-ray magnetic circular dichroism of individual magnetosomes by Scanning Transmission X-ray Microscopy, *Chemical Geology* 270, 110-116.
- Lefèvre, C. T., & Bazylinski, D. A. (2013). Ecology, diversity, and evolution of magnetotactic bacteria. *Microbiol. Mol. Biol. Rev.*, 77(3), 497-526.
- Le Nagard, L. , Zhu, X.H. , Hitchcock, A.P., Bazylinski, D.A., Swaraj, S., Stanescu, S., Belkhou, R. (2018a) How do Magnetotactic Bacteria Synthesize Magnetite? – a Soft X-ray Spectroscopy, Spectromicroscopy and Magnetism Time Course Study, *Microscopy & Microanalysis* 24, 376-377.
- Le Nagard, L., Morillo-López, V, Fradin, C. Bazylinski, D.A. (2018b), Growing Magnetotactic Bacteria of the Genus *Magnetospirillum*: Strains MSR-1, AMB-1 and MS-1, *JOVE* 140, DOI: 10.3791/58536
- Lerotic, M., Jacobsen, C., Gillow, J.B., Francis, A.J., Wirick, S., Vogt, S., Maser J. (2005) Cluster analysis in soft X-ray spectromicroscopy: Finding the patterns in complex specimens, *J. El. Spec. Rel. Phen.* 144, 1137-1143.
- Li, J., Pan, Y.X. , Chen, G., Liu, Q., Tian, L.X., Lin , W. (2009) Magnetite magnetosome and fragmental chain formation of *Magnetospirillum magneticum* AMB-1: Transmission electron microscopy and magnetic observations, *Geophys. J. Int.* 177, 33-42.
- Li, J., Benzerara, K., Bernard, S., Beyssac, O.(2013) The link between biomineralization and fossilization of bacteria: Insights from field and experimental studies, *Chemical Geology* 359, 49-69.
- Lin, W., Bazylinski, D.A., Xiao, T., Wu, L.-F., Pan, Y., (2014) Life with compass: diversity and biogeography of magnetotactic bacteria, *Environmental Microbiology* 19, 2646-2658.
- Lin, W., Paterson, G.A., Zhuc Q., Wang, Y., Kopylova, E., Lie, Y., Knight, R., Bazylinski, D.A., Zhuh, R., Kirschvink, J.L., Pan, Y. (2017) Origin of microbial biomineralization and magnetotaxis during the Archean, *Proc Natl Acad Sci U S A.* 114, 2171-2176.

- Marcano, L., García-Prieto, A., Muñoz, D., Barquín, L. F., Orue, I., Alonso, J., Muella, A., Fdez-Gubieda, M.L. (2017). Influence of the bacterial growth phase on the magnetic properties of magnetosomes synthesized by *Magnetospirillum gryphiswaldense*. *Biochimica et Biophysica Acta (BBA)-General Subjects*, 1861(6), 1507-1514.
- Miot, J., Benzerara, K., Morin, G., Kappler, A., Bernard, S., Obst, M., Férard, C., Skouri-Panet, F., Guigner, J.-M., Posth, N., Galvez, M., Brown Jr, G.E. Guyot, F. (2009) Iron biomineralization by anaerobic neutrophilic iron-oxidizing bacteria, *Geochimica et Cosmochimica Acta* 73, 696–711.
- Nagasaka M, Yuzawa, H., Horigome, T., Hitchcock, A.P., Kosugi, N. (2013) Electrochemical reaction of aqueous iron sulfate solutions studied by Fe L-edge soft X-ray absorption spectroscopy. *J Phys Chem C* 117(32): 16343–16348.
- Murat D., Falahati V., Bertinetti L., Csencsits R., Körnig A., Downing K., Faivre D., Komeili A. (2012) The magnetosome membrane protein, MmsF, is a major regulator of magnetite biomineralization in *Magnetospirillum magneticum* AMB-1, *Molecular Microbiology* 85, 684-699.
- Rivas-Lamelo, S., Benzerara, K., Lefèvre, C., Monteil, C., Jézéquel, D., Menguy, N., Viollier, E., Guyot, F., Férard, C., Poinso, M., Skouri-Panet, F., Trcera, N., Miot, J., Duprat, E. (2017) Magnetotactic bacteria as a new model for P sequestration in the ferruginous Lake Pavin. *Geochemical Perspectives Letters*, 5, 35-41.
- Scheffel, A., Gruska, M., Faivre, M., Linaudis, A., Plitzko, J.M., Schüler, D. (2006) An acidic protein aligns magnetosomes along a filamentous structure in magnetotactic bacteria. *Nature*, 440, 110-114.
- Schulz-Vogt H.N., Pollehne F., Jürgens K., Arz H.W., Beier S., Bahlo R., Dellwig O., Henkel J.V., Herlemann D.P.R., Krüger S., Leipe T., Schott T. (2019) Effect of large magnetotactic bacteria with polyphosphate inclusions on the phosphate profile of the suboxic zone in the Black Sea. *ISME J.* 13, 1198-1208.
- Staniland, S., Ward, B., Harrison, A., van der Laan, G., Telling, N. (2007) Rapid magnetosome formation shown by real-time x-ray magnetic circular dichroism, *Proc. Nat. Acad. Sci.* 104, 19524-19528.
- Swaraj, S., Belkhou, R., Stanescu, S., Rioult, M., Besson, A., Hitchcock, A.P. (2017) Performance of the HERMES beamline at the carbon K-edge, *IOP Conference Series: J. Phys. Conf. Series* 849, 012046
- Tanaka, M., Nakata, Y., Mori, T., Okamura, Y., Miyasaka, H., Takeyama, H., Matsunaga, T. (2008) Development of a Cell Surface Display System in a Magnetotactic Bacterium, “*Magnetospirillum magneticum*” AMB-1. *Applied and Environmental Microbiology* 74, 3342-3348.

- Thibault, P., Guizar-Sicairos, M., Menzel, A. (2014) Coherent imaging at the diffraction limit J. Synchrotron Rad. 21, 1011–1018.
- Wang, Y., Lin, W., Li, J., Pan, Y. (2013) Changes of cell growth and magnetosome biomineralization in *Magnetospirillum magneticum* AMB-1 after ultraviolet-B irradiation, Frontiers in Microbiology, Intracellular Biomineralization in Bacteria (eds. Lin, W., Benerara, K., Faivre, D. Pan, Y.)
- Wen, T., Zhang, Y., Geng Y., Liu, J., Basit, A., Tian, J., Li, Y., Li, J., Ju, J., Jiang, W. (2019) Epsilon-Fe<sub>2</sub>O<sub>3</sub> is a novel intermediate for magnetite biosynthesis in magnetotactic bacteria, Biomaterials Research 23, 13 (1-7).
- Winklhofer M, Abracado LG, Davila AF, Keim CN, Lins de Barros HGP (2007) Magnetic optimization in a multicellular magnetotactic organism. Biophys. J. 92: 661–670.
- Wolin, E.A, Wolin, M.J., Wolfe, R.S. (1963) Formation of methane by bacterial extracts. J. Biological Chemistry, 238, 2882–2886.
- Zhu, X.H., Kalirai, S.S., Hitchcock, A.P. Bazylinski, D.A. (2015) What is the correct Fe L<sub>23</sub> X-ray absorption spectrum of magnetite?, J. Electron Spectroscopy and Rel. Phenom. 199, 19-26.
- Zhu, X. H., Hitchcock, A.P., Bazylinski, D.A., Denes, P., Joseph, J., Lins, U., Marchesini, S. , Shiu, H.-W., Tyliczszak, T., Shapiro, D.A. (2016) Measuring spectroscopy and magnetism of extracted and intracellular magnetosomes using soft X-ray ptychography, Proc. Nat. Acad. Sci 113, E8219- E8227.

## Figure Captions

**Figure 1** Schematic of XMCD as applied to magnetotactic bacteria. (a) 3D view for tilt = 0°, with the vector for circular right (CR) polarization along the X-ray propagation direction (black) and the sample with 3 possible in-plane magnetization vectors (red, blue - horizontal, green - vertical). (b) Top view for tilt = 0°. There is no XMCD signal since the dot product of the photon polarization and each of the sample magnetization vectors is 0. (c) 3D view for polar angle tilt of 30°. (d) Top view for tilt = 30°. There is a 50% XMCD signal with both parallel (red) and antiparallel (blue) alignment of an in-plane, horizontal sample magnetization. If the sample magnetization is vertical (green) no XMCD would be observed at any polar tilt angle.

**Figure 2** (a) Images of particles in individual cells from the 9 time course points of batch B. In each case the image is  $OD_{\text{peak}} - OD_{\text{pre}}$  where  $OD_{\text{peak}}$  is average of 8 images from 707.5 to 711.5 eV, and  $OD_{\text{pre}}$  is average of 8 images from 702 to 706 eV. Scale bar is 200 nm in each case. (b) Fe L<sub>3</sub> spectra of particles extracted from stacks measured on the cells in Fig 2a. The zero of each spectrum is indicated on the vertical axis. The OD/cm scaling is the same for each spectrum. The arrow indicates the shoulder at 708.4 eV, which is more prominent in the spectra of particles at the 10 m, 30 m and 2 h time course.

**Figure 3** (a) Stacked bar chart of the numbers and distribution of sizes of the particles per cell derived from TEM images at each of the 9 time course points (batch B). The protocols used to achieve an accurate and unbiased distribution are discussed in the text. (b) evolution of numbers of particles within particle size ranges as a function of log(time). There is a 30 m lag phase followed by logarithmic growth of particles. Error bars not included for clarity. The corresponding numerical data, including standard deviation, are shown in Table S-2.

**Figure 4** (a) Average of 36 optical density (OD) images from 704 to 717 eV of an AMB-1 cells from a high Fe content culture of AMB-1 grown over an extended time period. The polarization was circular right (CR) and the sample was tilted 30° relative to the X-ray beam. The numbers at the right side of the image are the OD limits of the grey scale. (b) Color coded composite of component maps derived from a fit of the Fe L<sub>3</sub> stack to spectra for parallel (red), antiparallel (blue) magnetite and the no-Fe signal of the non-magnetite cell contents (green). The arrows indicate the directions of the parallel and antiparallel magnetic orientation. (c) Plot of the average Fe L<sub>3</sub> spectra of all the parallel (red) or anti-parallel (blue) magnetosomes, along with the derived X-ray magnetic circular dichroism (XMCD), as points. The solid lines are the spectra and XMCD reported for synthetic magnetite (Goering *et al.* 2007), scaled to match the optical density. The reference XMCD spectra was divided by 2 since at 30° tilt angle only 0.5 of the magnetic moment is projected on to the photon spin vector.

**Figure 5** (a) Fe map of the 8 h sample from batch A from difference of OD images at 709.2 and 700 eV. The rectangles identify precursor (green), intermediate (cyan) and fully formed (red & blue) magnetosomes. (b) XAS spectra recorded with CR of regions identified in (a), plotted on an absolute OD scale without offsets. (c) rescaled and offset plots of the same data, compared to the Fe L<sub>3</sub> spectra of FeCl<sub>3</sub> and the spectra of magnetite recorded with parallel and antiparallel circular polarization (Goering et al 2007). When dots and lines are superimposed (middle chain, precursor chain), the dots are the experimental data while the solid lines are a smoothed version as a ‘guide to the eye’. The other solid lines correspond to unsmoothed experimental data and reference spectra. The good agreement of the spectrum of the big magnetosome with the anti-parallel spectrum of magnetite and that of the left chain with that of the parallel spectrum of magnetite shows that the magnetization vector of the big magnetosome and that of the left chain are oriented in opposite directions. The feature at 708.4 eV is strongest in the precursor chain (green) but is weak or absent in the other two chains, indicating a transition from Fe(III) to pure magnetite.

**Figure 6** Analysis of a cell from 5.7 h sample, batch B. (a,b) TEM images measured after the STXM measurements. (c) Average of all images of the Fe L<sub>3</sub> stack measured with CR with the sample at a tilt angle of 0°. (d) XMCD map (OD<sub>708.2</sub>-CR - OD<sub>708.2</sub>-CL) measured with the sample at a tilt angle of 0°. (e) XMCD map (OD<sub>708.2</sub>-CR - OD<sub>708.2</sub>-CL) measured with the sample at a tilt angle of 30°. (f) Fe L<sub>3</sub> XAS and XMCD spectra of all the black particles in Fig. 5e, measured with the sample at a tilt angle of 30°.

**Figure 7** Fe L<sub>3</sub> spectra extracted from an Fe L<sub>3</sub> stack of the 24 h AMB-1 sample from batch B, measured with CR at a tilt angle of 30°. These five spectra were used to fit the stack, so as to obtain the component maps presented in Figure 8.

**Figure 8** 24 h sample from batch B, measured with the sample plate tilted at 30°. (a) image of complete cell at 709.7 eV. (b) average of all 60 images of stack recorded in the top half of the cell. Component maps derived from a 5-component fit of the Fe L<sub>3</sub> image sequence (spectra shown in Fig. 7) of (c) cell, (d) Fe(III), (e) magnetosomes with antiparallel spectra in CR, (f) magnetosomes with parallel spectra in CR, (g) ‘rim’ signal, showing a band of Fe-containing material along the outer boundaries of the expanded part of the cell (bright in Fig. 8c). This spectral component also maps signals in the magnetosome chain. See Fig. S-5 for results of an alternate fit. (h) color coded composite of maps of the antiparallel (red), cell (green) and parallel (blue) component maps.

**Figure 9** Fe L<sub>3</sub> spectra of the magnetosomes in the 24 h AMB-1 cell of batch B recorded with CR and CL with the sample tilted at 30°. The resulting XMCD signal is also plotted. In each case the data from the magnetosomes of the cell from the 24 h sample is overplot with the corresponding spectra from pure magnetite (Goering et al, 2007).



**Graphical Abstract**

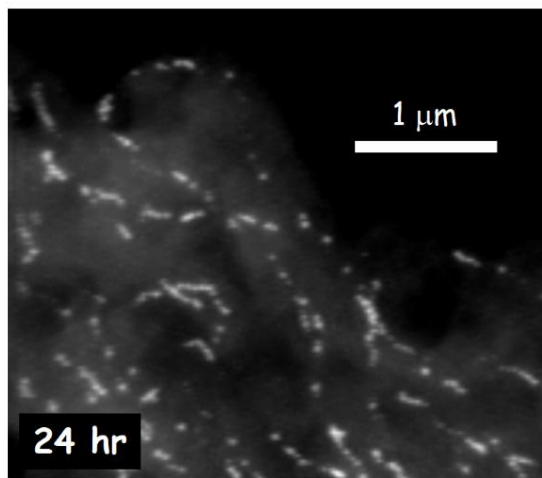
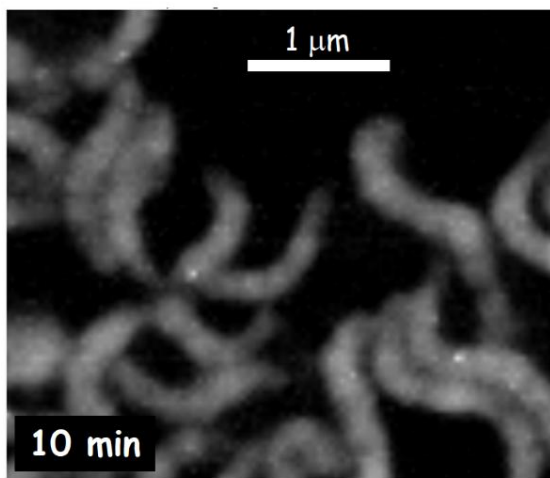


Figure 01  
[Click here to download high resolution image](#)

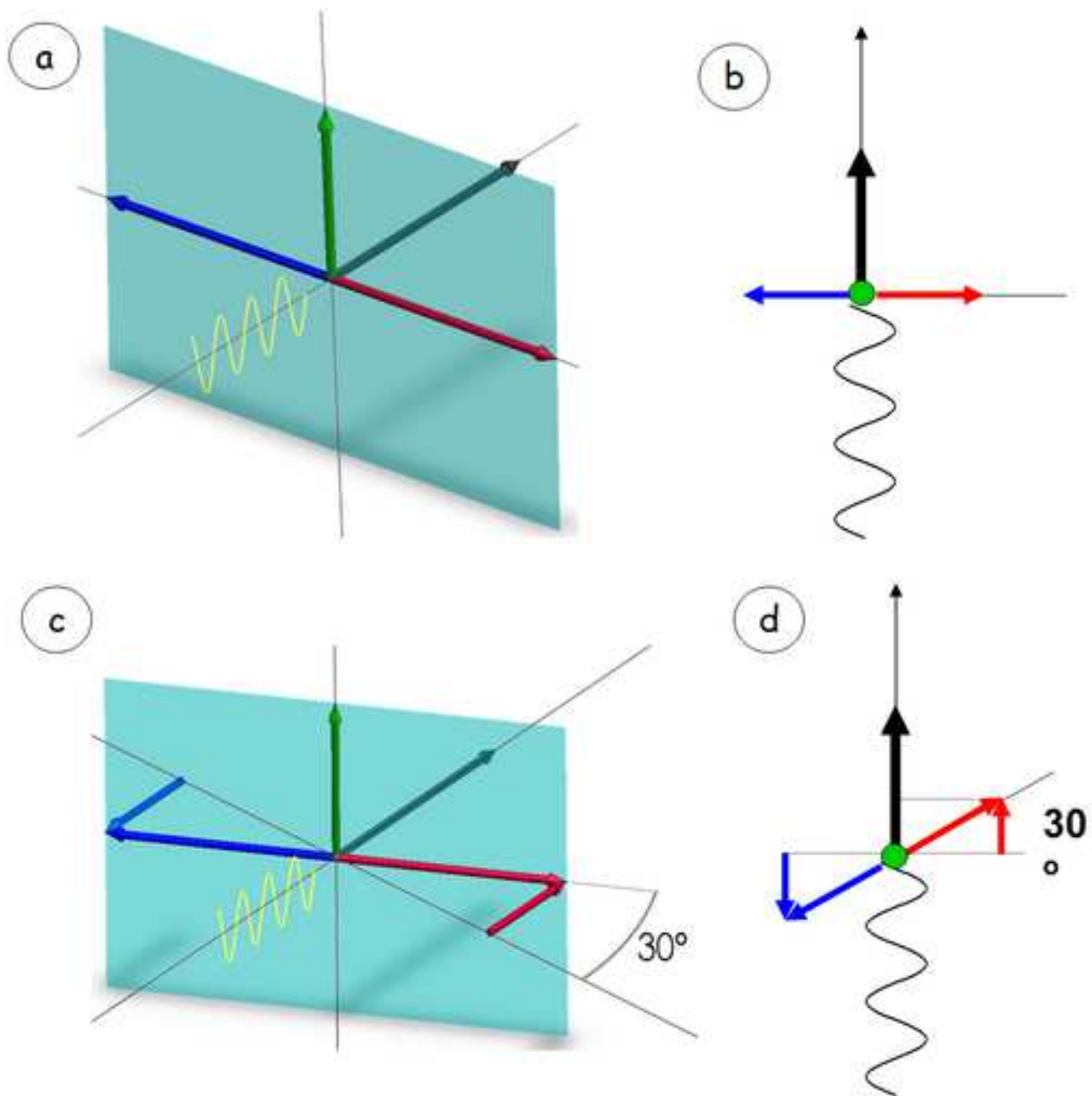


Figure 02  
[Click here to download high resolution image](#)

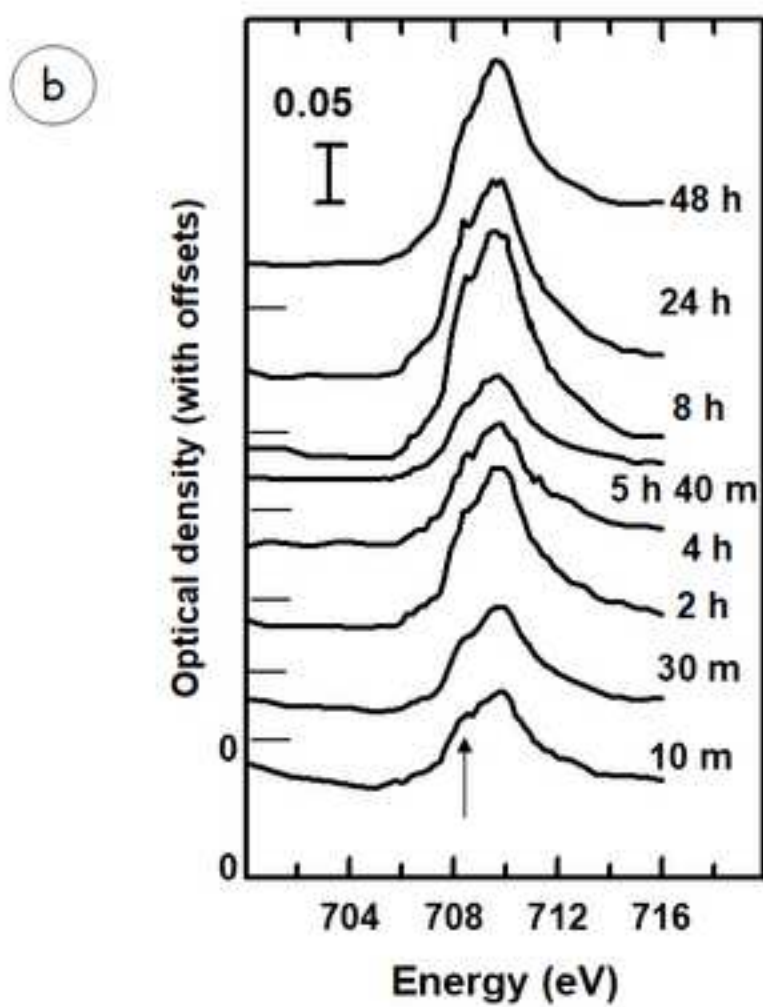
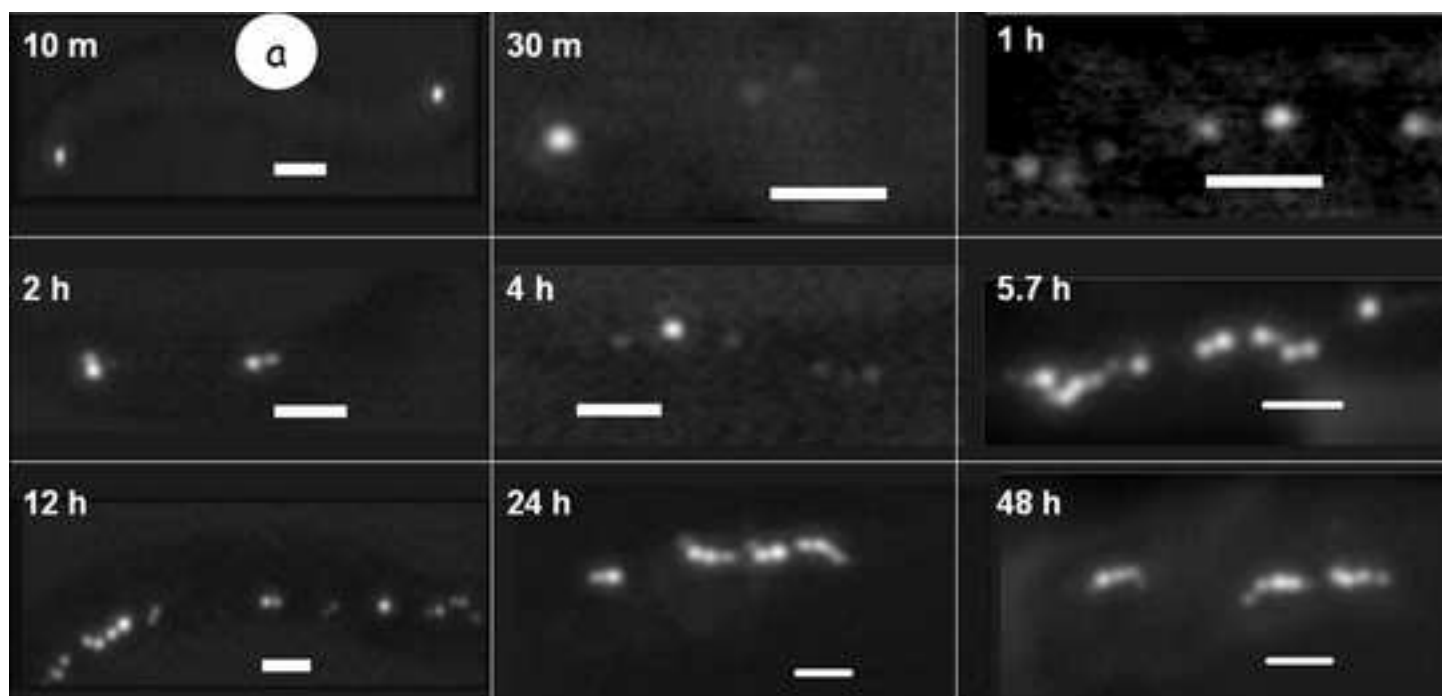


Figure 03  
[Click here to download high resolution image](#)

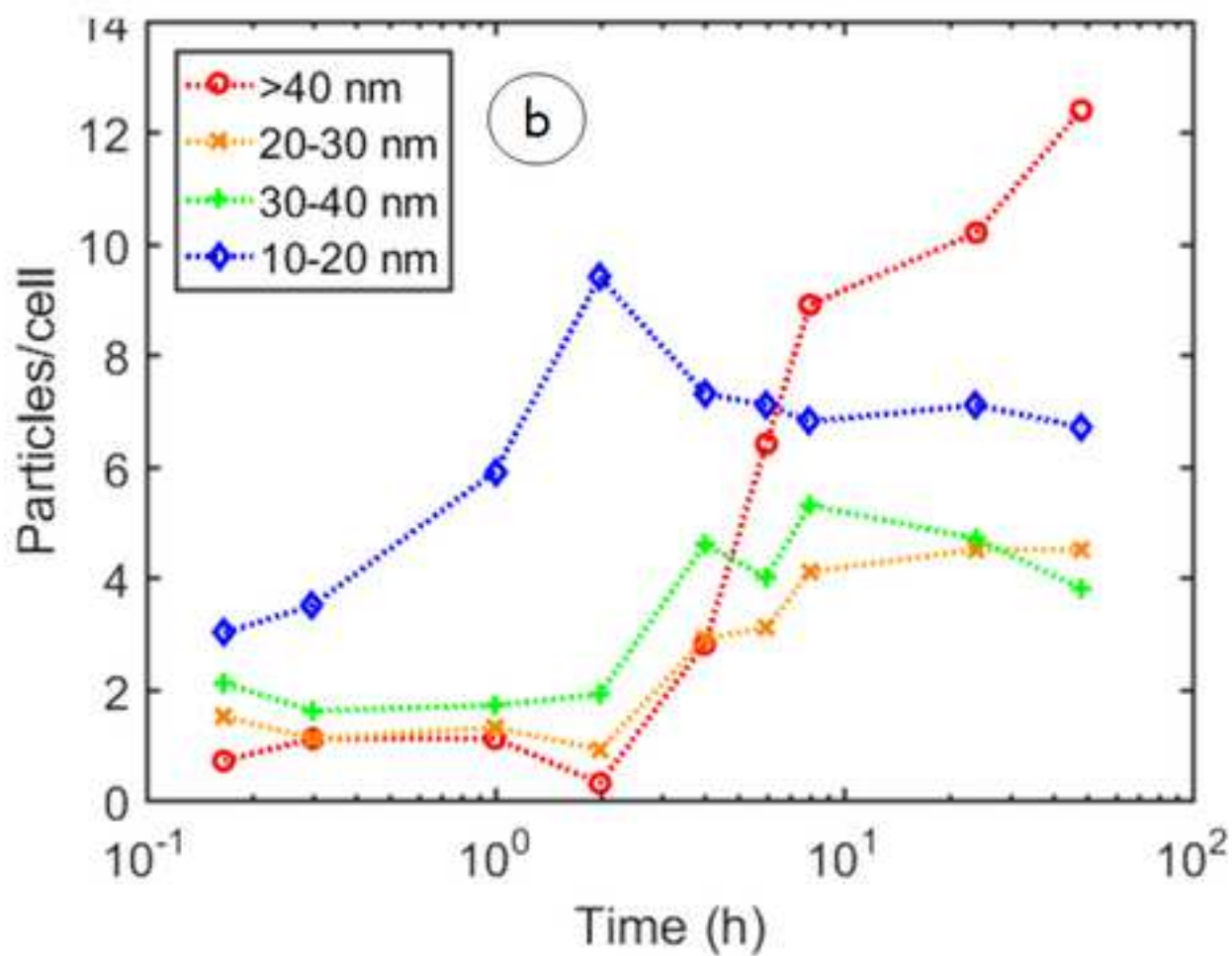
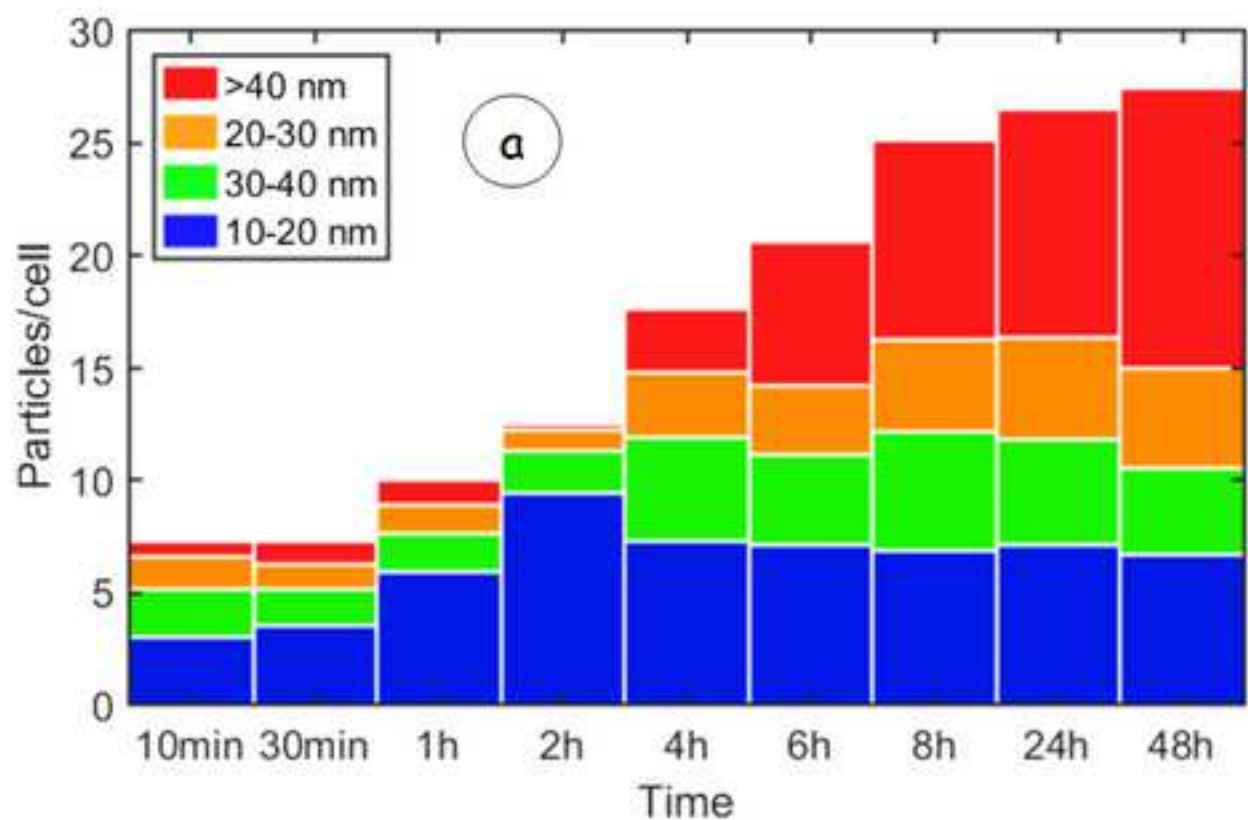


Figure 04

[Click here to download high resolution image](#)

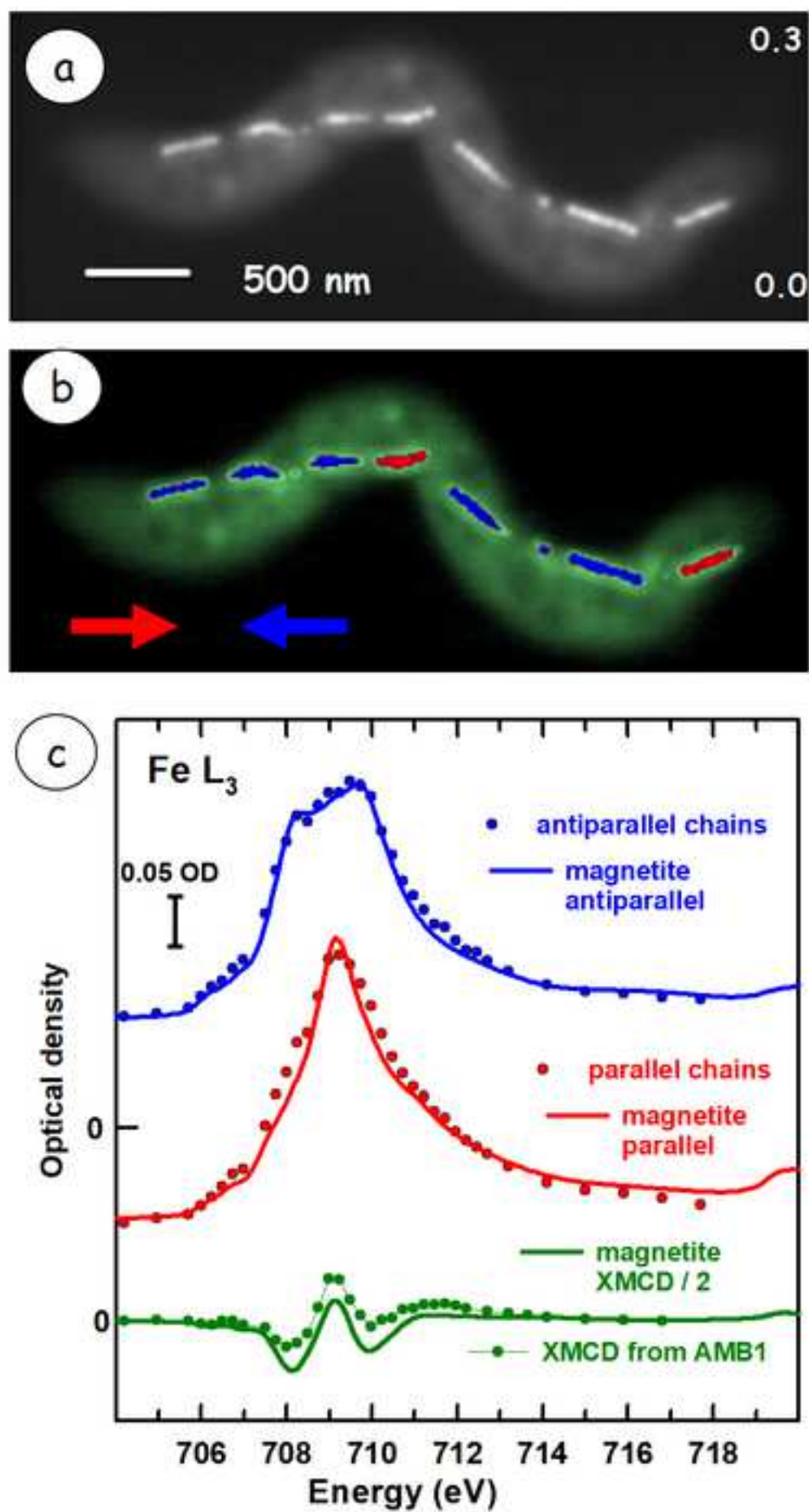




Figure 05  
[Click here to download high resolution image](#)

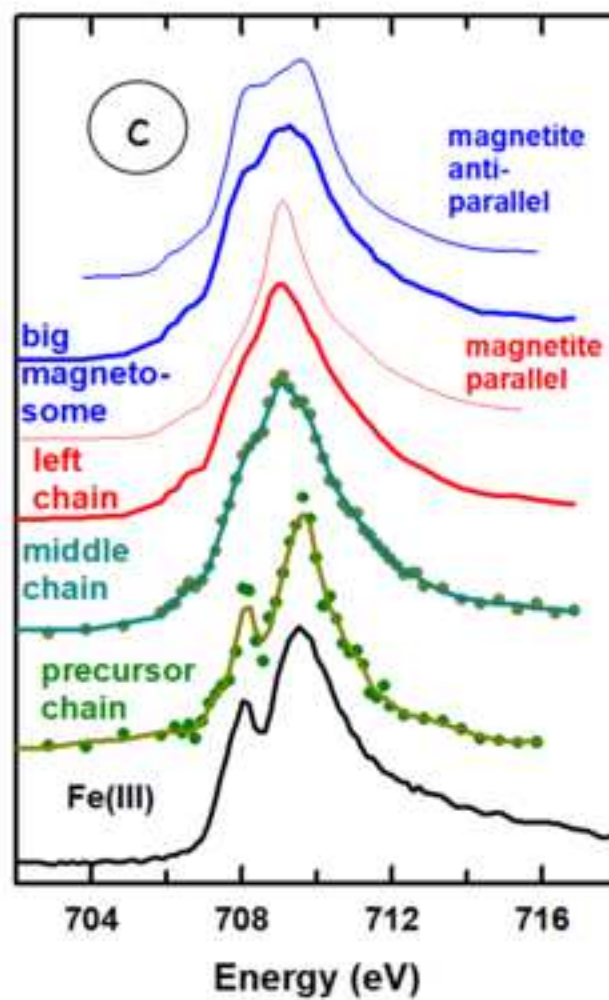
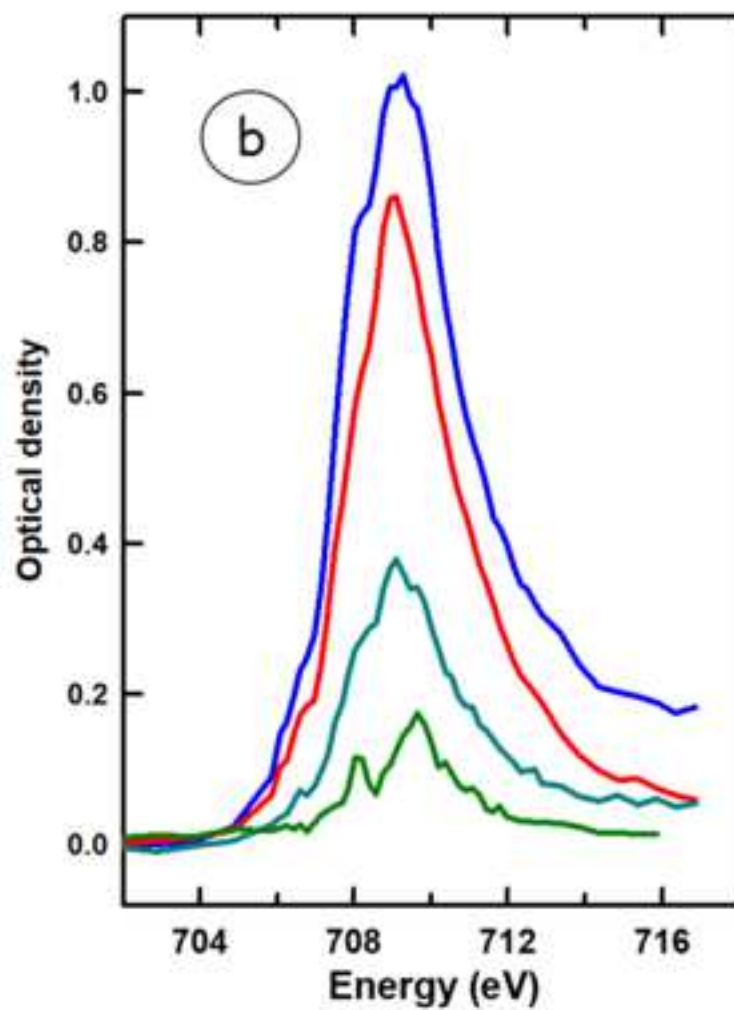
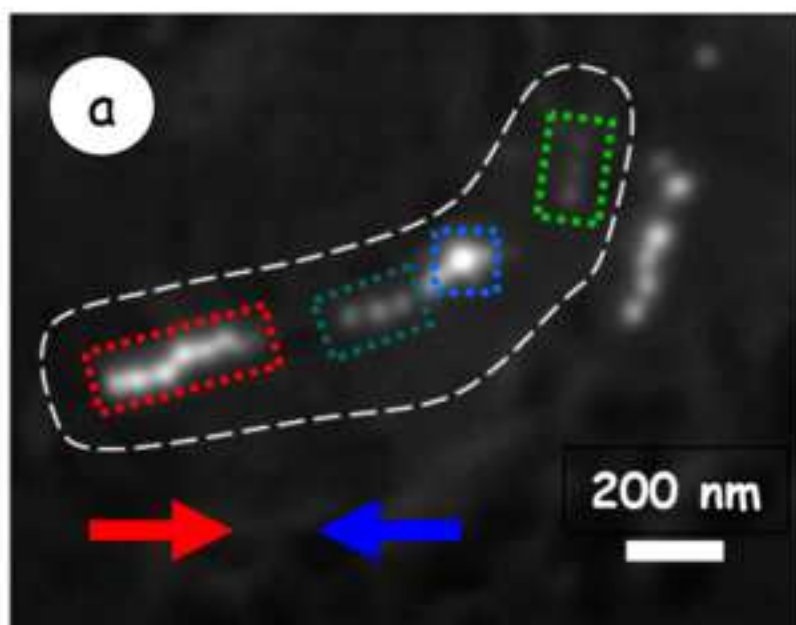


Figure 06

[Click here to download high resolution image](#)

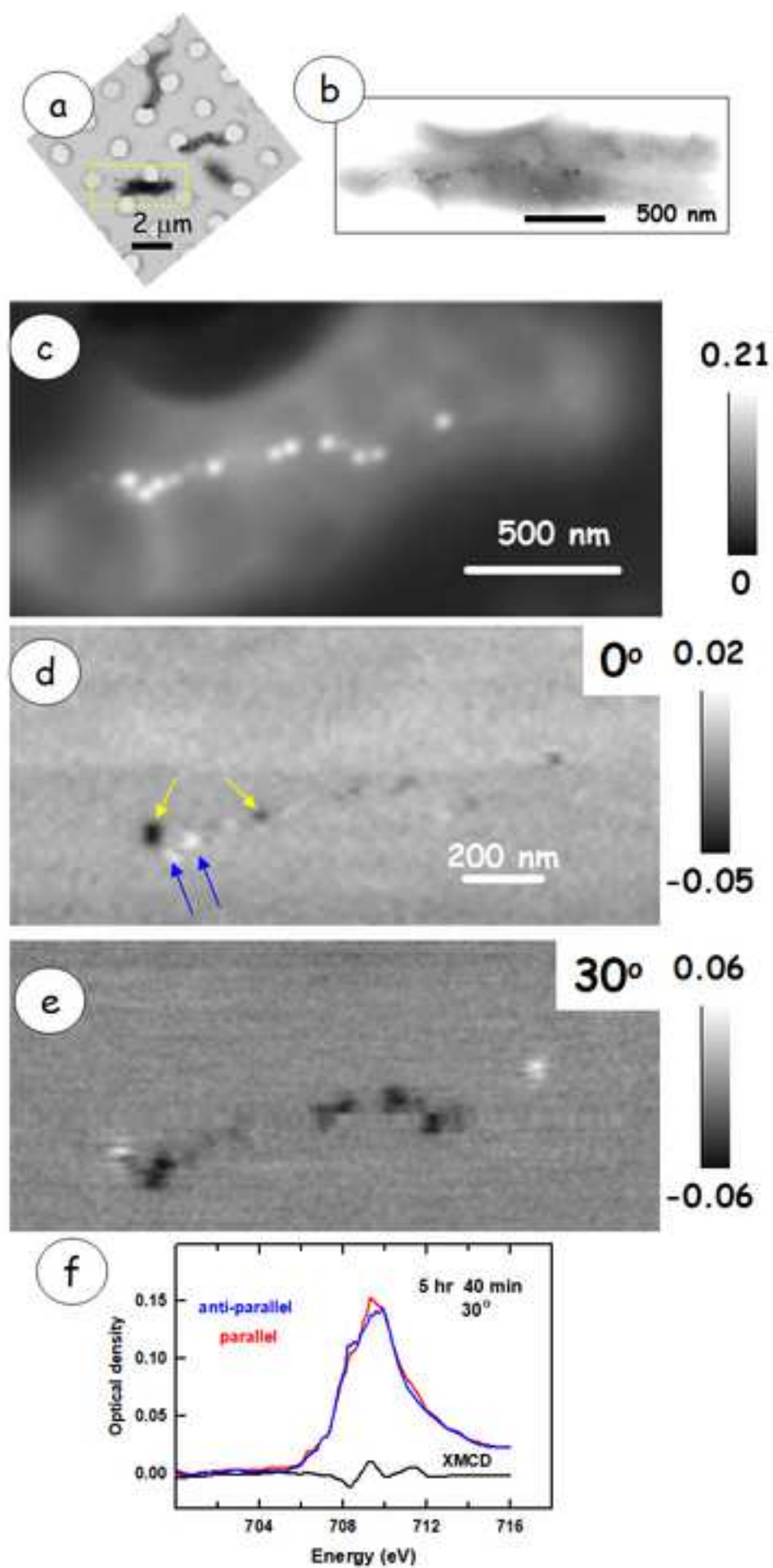


Figure 07  
[Click here to download high resolution image](#)

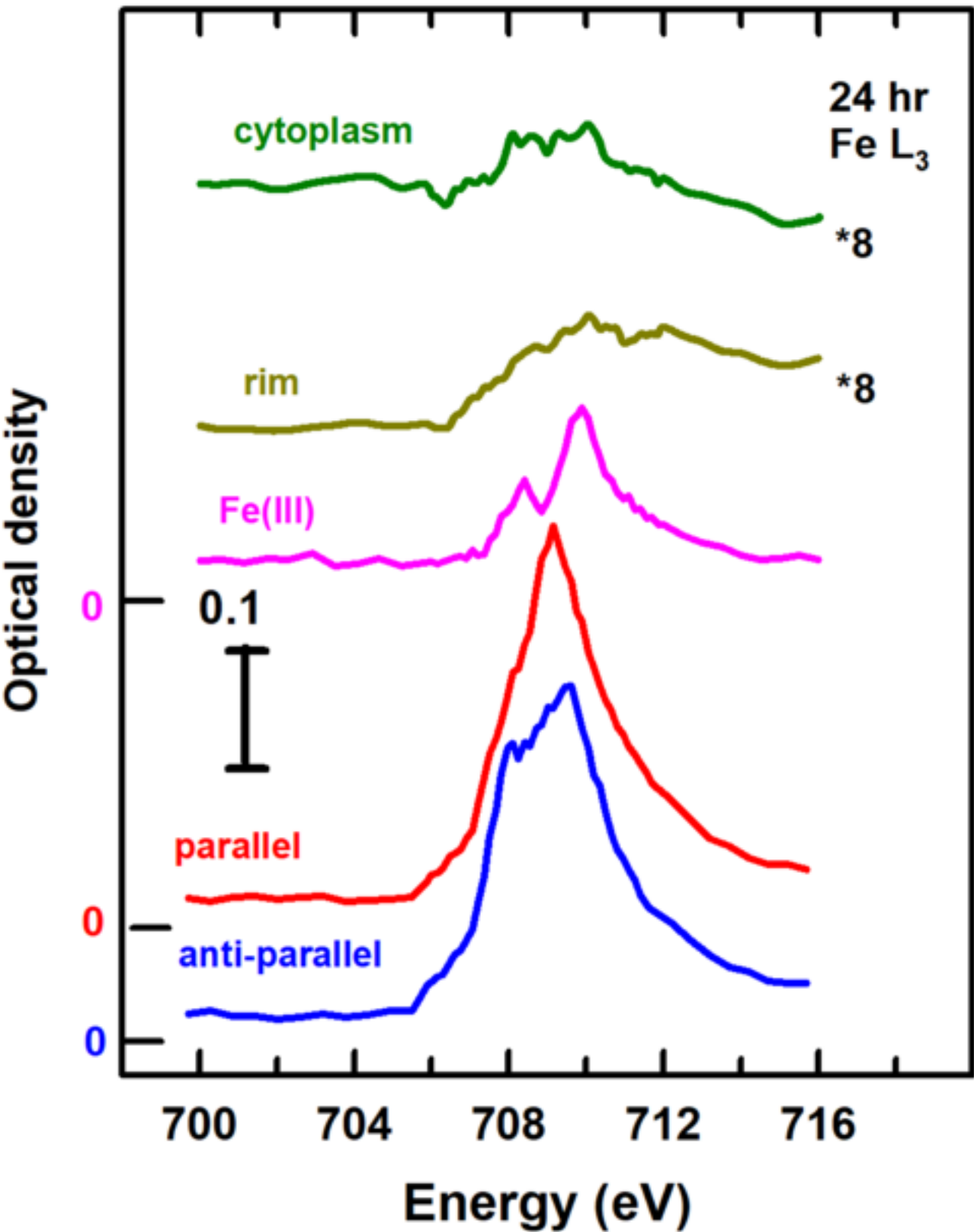




Figure 08  
[Click here to download high resolution image](#)

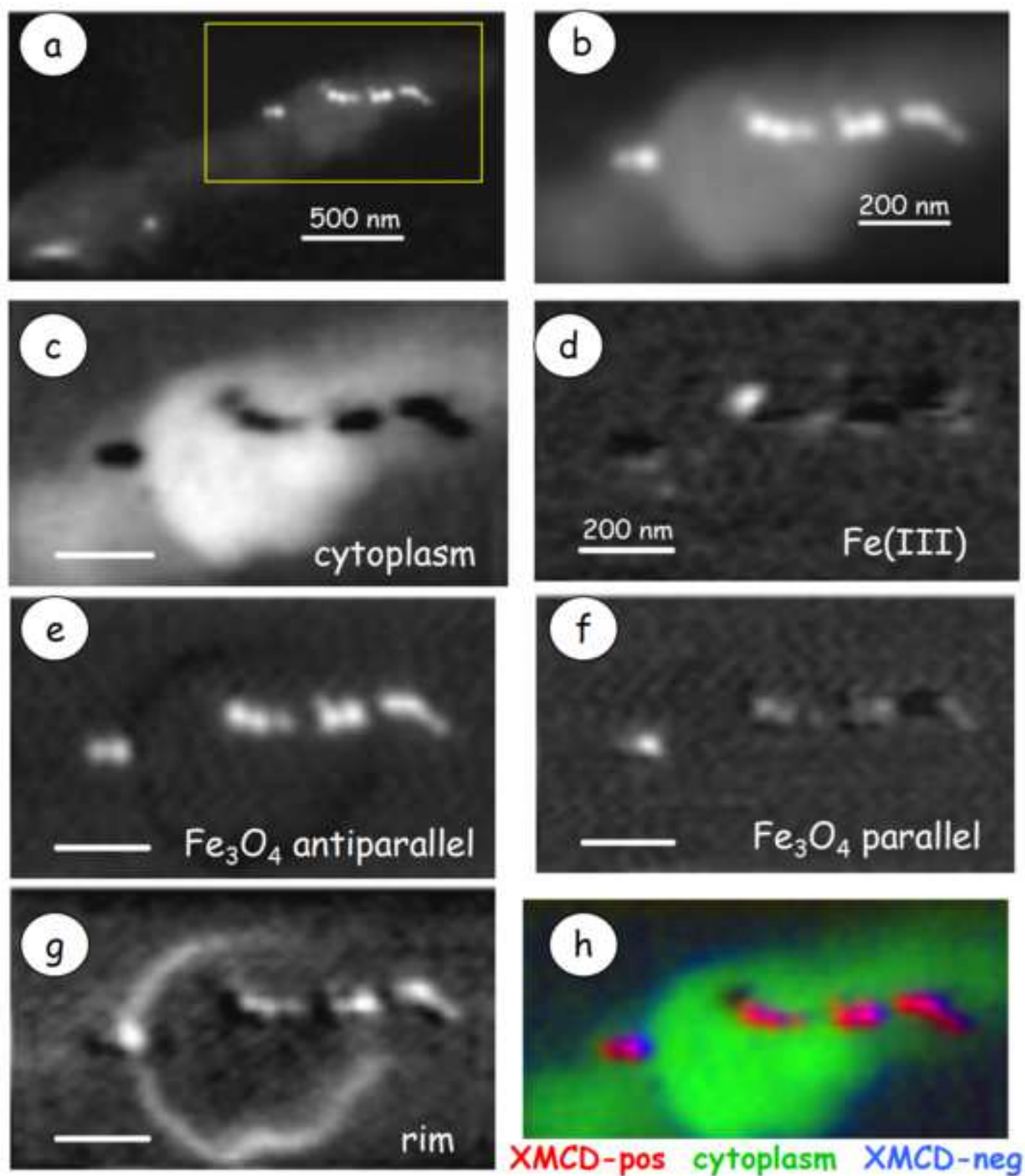
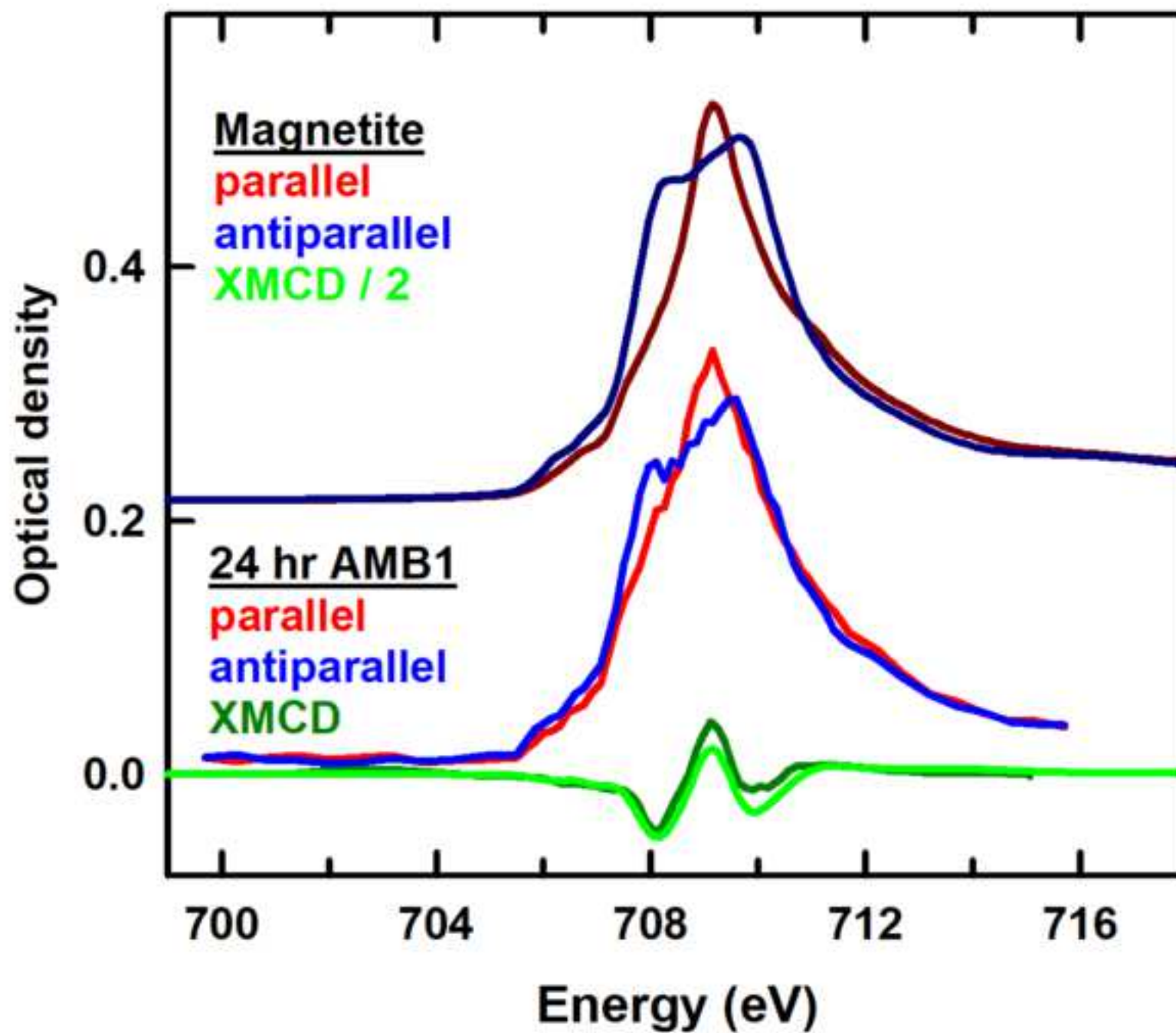


Figure 09

[Click here to download high resolution image](#)



**Supplementary information file**

**[Click here to download Background dataset for online publication only: AMB1-time-course-STXM-SI-revised-submitted.pdf](#)**